Current Pollution Reports
https://doi.org/10.1007/s40726-020-00158-0

AIR POLLUTION (H ZHANG AND Y SUN, SECTION EDITORS)

Recent Progress in Impacts of Mixing State on Optical Properties of Black Carbon Aerosol

Xiaodong Wei[1,2,3,4] · Yanhong Zhu[1] · Jianlin Hu[1] · Chao Liu[5] · Xinlei Ge[1] · Song Guo[6] · Dantong Liu[7] · Hong Liao[1] · Huijun Wang[2,3]

Abstract

Black carbon (BC) exerts profound impacts on air quality and climate because of its high-absorption cross section over a broad band of solar spectrum. Non-BC materials coated on BC could alter the mixing state of BC particles and can considerably enhance its mass absorption coefficient. Quantification of this absorption enhancement remains a challenge due to incomplete understanding of the complex physical and chemical properties related to mixing states. In this paper, we summarize the recent progress in measurement and modeling studies on the BC mixing state and their effects on optical properties. Laboratory and field-based observations have shown that the transformation of a mixing state from a highly fractal nature to a more compact shape exhibits a decrease in electric mobility diameter but an increase in fractal dimension and effective density. Meanwhile, the transition behavior is also obviously influenced by emission source which can determine the components of BC mixtures. Based on the empirically determined parameters, accurate numerical modeling shows great capability on calculating BC optical properties. However, considering the significant uncertainties related to BC microphysical properties, proper parameterization considering realistic BC aggregates and coating fraction can help to understand the progress from an externally to internally mixed state.

Keywords Black carbon · Mixing state · Optical properties · Absorption enhancement · Optical model

Introduction

Black carbon (BC, also known as soot) is a distinct type of carbonaceous aerosols, which has a unique combination of properties, including strong visible light absorption of at least 5 m^2/g at 550 nm [1], aggregate morphology [2], refractory with vaporization temperature near 4000 K [3], and insolubility in water and common organic solvents [4]. The absorption spectrum of BC aerosols is wider than that of typical greenhouse gases such as CO_2 and CH_4, with a strong absorption effect on solar radiation from infrared to ultraviolet wavelengths [5, 6]. However, unlike the long timescale associated

This article is part of the Topical Collection on *Air Pollution*

✉ Jianlin Hu
jianlinhu@nuist.edu.cn

[1] Jiangsu Key Laboratory of Atmospheric Environment Monitoring and Pollution Control, Collaborative Innovation Center of Atmospheric Environment and Equipment Technology, School of Environmental Science and Engineering, Nanjing University of Information Science & Technology, 219 Ningliu Road, Nanjing 210044, China

[2] Collaborative Innovation Center on Forecast and Evaluation of Meteorological Disasters/Key Laboratory of Meteorological Disaster, Ministry of Education, Nanjing University of Information Science and Technology, Nanjing 210044, China

[3] Nansen–Zhu International Research Centre, Institute of Atmospheric Physics, Chinese Academy of Sciences, Beijing 100029, China

[4] East China Air Traffic Management Bureau CAAC, Shanghai 200335, China

[5] Key Laboratory for Aerosol-Cloud-Precipitation of China Meteorological Administration, School of Atmospheric Physics, Nanjing University of Information Science & Technology, Nanjing 210044, China

[6] State Key Joint Laboratory of Environmental Simulation and Pollution Control, College of Environmental Sciences and Engineering, Peking University, Beijing 100871, China

[7] Department of Atmospheric Science, School of Earth Sciences, Zhejiang University, Hangzhou 310027, China

Published online: 17 August 2020

with the removal of CO_2, the atmospheric lifetime of BC aerosols is relatively short, typically of the order of 1 week [7, 8]. Thus, BC is considered as a short-lived climate forcer (SLCF) and studies suggest that BC is the second most important global warming factor only after carbon dioxide [9, 10].

BC is produced from incomplete fossil fuel combustion, automobile and aircraft emissions, and biomass burning. Freshly generated BC particles are hydrophobic and bare of any nonrefractory material and exist as an external mixture in which strongly light-absorbing BC and organic and inorganic light-scattering components reside in different particles [11, 12]. Once emitted into the atmosphere, the morphology of emitted chain-like aggregates changes rapidly with the diffusion, transport, and collision in the atmosphere [13]. Meanwhile, BC particles undergo aging processes through the uptake of reactive gases, such as OH, O_3, NO_2, NO_3, N_2O_5, HNO_3, and H_2SO_4 [8–11]. Consequently, such particles gradually become internally mixed and are no longer pure BC but contain nitrate, sulfate, and secondary organic matter [11, 14]. Because BC is insoluble, it is always distinctly separated from the other material in an internally mixed particle. The presence, relative quantities, and location of non-absorbing materials in BC-containing particles require a complex characterization commonly summarized in the single term of "mixing state" [5].

Recent observational and modeling studies have indicated that mixing state and material compositions can obviously change the optical properties of BC aerosols [15–19]. In the early 2000s, a few studies [9, 20, 21] pointed out that the aging processes could enhance absorption coefficients of solar radiation, which was called the "lensing effect." Many observational studies have revealed absorption enhancement in various locations around the world [14, 22, 23]. However, there are significant differences in the reported absorption enhancement among the studies due to diversity in particle size, phase state, and chemical composition in the different regions [2, 24] and some studies reported no obvious changes in absorption coefficients [15].

Recognizing the important impact of mixing state on BC optical properties, recent studies have been conducted using several different methods including laboratory experiments, field measurements, and numerical modeling. The objective of this review is to summarize the progress made in the recent research (mostly after 2005) on the impacts of mixing state to BC optical properties. The remainder of this paper is organized as follows: "Measurements of BC Mixing States" discusses the measured morphologic parameters related to mixing state; "Measurements of BC Optical Properties" presents the studies measuring the BC optical properties; "Modeling of BC Mixing States and Optical Properties" summarizes the progress made in numerical modeling BC mixing states and optical properties; and finally we summarize the major findings in recent studies and make recommendations for future studies.

Measurements of BC Mixing States

Information about the mass and size of BC core, coating materials, and morphology is needed to determine the BC mixing state. Traditional optical-based methods and thermal-based methods [25, 26] have difficulty in isolating BC from the coating components with which it is internally or externally mixed. With the development of instruments, two kinds of real-time instrumental techniques make important contributions toward quantifying the mixing state of BC-containing particles. The Single Particle Soot Photometer (SP2) provides refractory black carbon (rBC) mass loadings, particle number concentrations, and size distribution measurements for research of BC mixing states [27, 28]. The Soot Particle Aerosol Mass Spectrometer (SP-AMS) is an AMS equipped with an intracavity laser vaporizer (1064 nm) based on the SP2 design, which can exclusively determine the BC-containing particles, and characterize the size distributions as well as chemical compositions of BC cores and the coating materials [29]. Electron microscopy can provide accurate morphology of soot aggregates, showing that the graphitic spherules coagulate to form aggregates or fractal chain-like structures consisting of hundreds or thousands of spherules [11]. Techniques using the filter-based approach including the Particle Soot Absorption Photometer (PSAP) and Multi-Angle Absorption Photometer (MAAP) are commonly used to measure the absorption enhancement of BC-containing particles, with the application of empirical corrections to overcome the bias caused by other light-absorbing aerosols [30]. Instruments that do not use filters are also available for the measurement of absorption by BC. In the photoacoustic spectrometer (PAS) [31], particles are drawn into an acoustic cavity and irradiated by power-modulated laser light. Based on the various measurements, the distinction of microphysical properties (i.e., morphologies and optical properties) for BC mixed with organic and inorganic (i.e., sulfate and nitrate) species can be quantified through parameters listed in Table 1.

Fractal Dimension

Fresh BC particles are common in the form of random aggregates, which can be described using the fractal concept. This concept is of value because it includes a mathematical description and a quantifiable parameter fractal dimension (D_f). The mathematical description is so-called scaling law as shown in

Table 1 Abbreviations and symbols quantifying microphysical properties of BC mixtures in literature

categories	Abbreviation/ symbols	Full name/explanation
Measurement instruments	AMS	Aerosol mass spectrometer
	APS	Aerodynamic particle sizer
	SP2	Single-particle soot photometer
	TEM/SEM	Transmission/scanning electron microscopy
	SP-AMS	Soot particle aerosol mass spectrometer
Mixing state	rBC	Refractory black carbon determined by the SP2 through the laser-induced incandescence method
	D_f	Fractal dimension
	D_a	Aerodynamic equivalent diameter selected by APS
	D_{mob}	Mobility diameter selected by the DMA
	D_{me}	Mass equivalent diameter of BC particles
	M_R	The mass ratio of coatings to BC particles
	ρ_{eff}	Effective density
	DSF	Dynamic shape factor of particles
Optical properties	MAC	Mass absorption cross section
	AAE	Absorption Ångstrom exponent
	E_{abs}	Absorption enhancement factor
	ω_0	Single-scattering Albedo

Eq. (1) [32], and the particles composing the aggregates are called "primary particles" or "monomers." Ideally, they are spherical with point contacts and all the same size.

$$\mathrm{N} = k_f \left(\frac{R_g}{\alpha}\right)^{D_f} \tag{1}$$

where N is the total number of monomers in each aggregate (proportional to the mass); a is the monomer radius; k_f is the fractal proportionality constant (also called fractal prefactor or structural coefficient); D_f is the fractal dimension, $D_f = 1$ indicates an unlimited straight line, and $D_f = 3$ means a sphere; the radius of gyration R_g is a measure of the overall aggregate radius and can be calculated by

$$R_g^2 = \frac{1}{N}\sum_{i=1}^{N}\left(\overrightarrow{r_i} - \overrightarrow{r_c}\right)^2 \tag{2}$$

where $\overrightarrow{r_i}$ and $\overrightarrow{r_c}$ denote the position vectors of the center of each monomer and aggregate mass center, respectively, and $\overrightarrow{r_c}$ can be calculated by

$$\overrightarrow{r_c} = \frac{1}{N}\sum_{i=1}^{N}\left(\overrightarrow{r_i}\right) \tag{3}$$

The value of k_f represents the level of compactness. For a given D_f, the smaller the prefactor value, the lower the packing density. The method using electron tomography to select D_f and k_f is not commonly available, which requires a sophisticated system of transmission electron microscopy. For most studies, D_f and k_f can be estimated from a power-law fit of a scatter plot of N versus the values of R_g/a [13, 33–35].

The value of D_f can vary largely depending on emission sources and aging processes (Fig. 1). Due to the limitation of the sampling method, most studies cannot capture the values during the whole aging processes. Figure 1 shows the published D_f data. D_f is obviously smaller at externally mixed states than that at internally mixed states. Specifically, the range of external mixture values is 1.53–1.83 [13, 33–41] but increases to 1.86–2.16 [13, 34, 35, 42, 43] after an internal mixture with other aerosol components. BC from internal combustion engines can become thickly coated with condensable material (e.g., sulfate and nitrate salts) after hygroscopic growth (Fig. 1b), and a large amount of directly emitted organic matter (including both primary and secondary aerosol) is internally mixed with BC from sources such as wildfire combustion (Fig. 1a). Traffic-emitted BC mixtures have a higher value than wildfire emissions after atmospheric aging. Figure 1 also indicates that few observations show that the value of D_f can reach 3, therefore the core–shell assumption requiring BC to be spherical is inconsistent with actual morphologies.

Equivalent Diameters

When the physical characteristics (e.g., volume, mass, and terminal velocity) of BC aggregates are identical with those of spherical BC particles, the spherical diameters are called equivalent diameters. The equivalent diameters can be specifically divided into the following categories, reflecting the

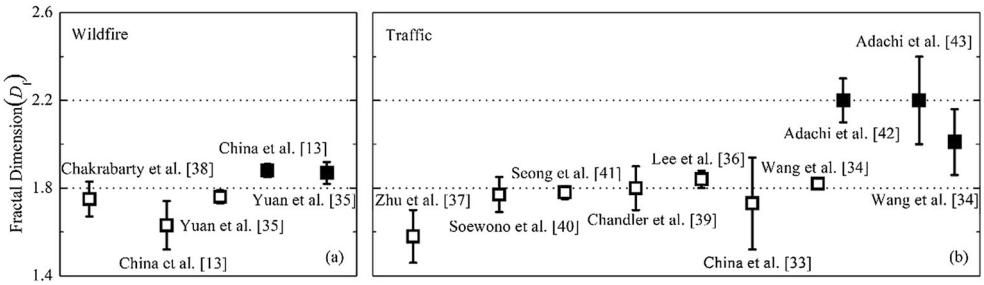

Fig. 1 Fractal dimension (D_f) of previously published data. The hollow and solid symbols represent the externally and internally mixed BC particles. The error bars represent 2σ uncertainty

particle sizes and mixing state according to the measurement principle. The vacuum aerodynamic diameter (D_a) is widely applicable to the AMS (aerosol mass spectrometer) measurement, defined as the diameter of a sphere with a standard density that settles at the same terminal velocity as the particle of interest and usually less than 100 nm for black carbon because of their formation mechanism [44]. It is an expression of aerodynamic behavior of an irregularly shaped particle in terms of the diameter of an idealized particle. Then, particles having the same aerodynamic diameter may have different dimensions and shapes. Currently, freshly emitted BC particles demonstrate fractal chain-like structures consisting of hundreds or thousands of spherules [2, 11, 13, 34]. Due to the deficiency of D_a in characterizing the BC morphology and aging, mobility diameter (D_{mob}) and mass equivalent diameter (D_{me}) are often used in the application.

In practice, a differential mobility analyzer (DMA), aerosol particle mass (APM) analyzer, and condensation particle counter (CPC) are often integrated to obtain the BC mass (M_{BC}) and mobility diameter (D_{mob}) simultaneously [2, 45, 46]. Measurements of D_{mob} can directly reflect the compactness of BC particles as shown in Fig. 2. Smaller D_{mob} represents more compact in morphology with the same M_{BC}. Under the spherical assumption, D_{mob} equals D_{me} and D_a can be calculated by Eq. (4):

$$D_a = D_{mob} \times \sqrt{\rho_{BC}/\rho_0} \tag{4}$$

where ρ_{BC} is the material density (the density of particles with a solid spherical structure), which is different from the effective density to be discussed next, and ρ_0 is a constant equal to 1 g/cm^3. D_{mob} of a fractal-like agglomerate has a power-law relation to the BC mass as shown in Eq. (5) [47].

$$M_{BC} = \mathrm{C} \times (D_{mob})^{D_{fm}} \tag{5}$$

where coefficient C and mass-mobility scaling exponent D_{fm} can be obtained by fitting the measured M_{BC} and D_{mob} [2]. The term "fractal dimension" has not been used rigorously for the D_{fm} in a couple of studies [24, 48, 49]. Notably, though, the value of D_{fm} is not identical to the fractal dimension D_f described in "Fractal Dimension" due to different calculation principles [50].

The dynamic shape factor (DSF) evaluates the increase in drag force on a fractal BC particle compared with a spherical particle with the same equivalent volume when both are moving at the same speed [51, 52], calculated from the measured mobility diameter D_{mob} and the calculated volume equivalent diameter D_{ve}:

$$\mathrm{DSF} = \frac{D_{mob} C_{ve}}{C_p D_{ve}} \tag{6}$$

where C_{ve} and C_p are the Cunningham slip correction factors for particles with diameter D_{ve} and D_{mob}, respectively. The value of DSF represents an important parameter to

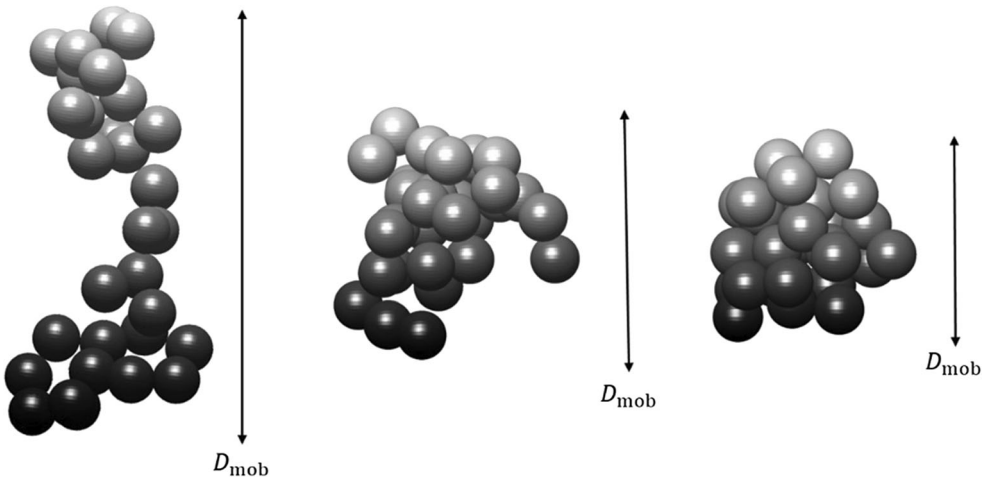

Fig. 2 A schematic of mobility diameter evolution reflecting the compactness of BC-containing particles

characterize the morphology of BC-containing particles; DSF = 1 means a spherical particle without cavities. Recent study [53] has shown that DSF decreases from 2.23 ± 0.29 at 300 nm D_{mob} to 1.60 ± 0.20 at 125 nm D_{mob} for diesel-emitted BC particles coated with organic materials. BC particles generated from incomplete combustion of propane have the value of DSF decreasing from 2.8 to 1.0 with organic coating processes [24, 54].

The change in the mass equivalent diameter ΔD_{me} (or total coating thickness) of BC particles can be directly derived from the total particle mass (M_p) and coating material density ($\rho_{non\text{-}BC}$), which are usually applicable to quantify the BC aging [15, 17, 24]. The mass ratio of non-BC matter to BC (M_R) is also used to discuss the aging process, and related to ΔD_{me} by Eq. (7):

$$M_R = \frac{\rho_{non-BC} \times \left[\left(D_{me,0} + \Delta D_{me}\right)^3 - \left(D_{me,0}\right)^3\right]}{\rho_{BC} \times \left(D_{me,0}\right)^3} \quad (7)$$

where $D_{me,0}$ is the initial mass equivalent diameter of BC particles. The value of M_R or ΔD_{me} shows wide-ranging results under various aging stages. M_R varies from about 0 to ~ 30 depending on the combustion source [17]. In contrast, $\Delta D_{me}/D_{me,0}$ changes from 0 to ~ 1.5 in Beijing [24], and the corresponding M_R is 0 to ~ 12 according to Eq. (7). It is difficult to distinguish aging stages and mixing states only depending on M_R or ΔD_{me}. The value of D_{mob} is intrinsically related to M_R or ΔD_{me} through the evolutions of effective density [45, 46], which is a key parameter relevant to the compactness. The morphology-independent measurement on BC mixing states has been achieved by measuring the rBC mass for the particle mass selected monodispered particles, where both particle mass and rBC mass could be quantified simultaneously [17]. In addition, combining with scattering cross-section measurement of a single BC particle, the volume ratio between coating and rBC could be obtained, and hereby integrated to also derive the coating volume ratio for bulk [55].

Effective Density

The effective density (ρ_{eff}) is defined as the ratio of the particle mass (M_p) to the volume of its mobility equivalent sphere:

$$\rho_{eff} = \frac{6M_p}{\pi D_{mob}^3} \quad (8)$$

The compactness of a particle can be determined by comparing the ρ_{eff} with the material density (the density of particles with a solid spherical structure). For particles with the same material density, a smaller ρ_{eff} indicates a looser structure. Measured ρ_{eff} values listed in Table 2 from recent literature [2, 17, 24, 46, 48, 49, 53, 54, 56–63] show great diversities with various emission sources and mixing states, and changes from 0.09 to 1.97 g/cm^3. Studies in urban environments (Tables 2) revealed obvious regional differences for both external and internal mixing states [56, 62, 63]. Externally to internally mixed BC particles exhibit a remarkable change in morphology, characterized by a decrease in D_{mob} but an increase in D_f and ρ_{eff}. The value of ρ_{eff} approaching the coating material density indicates complete transformation from highly fractal to fully compact and spherical BC particles [2, 46, 54]. Recent measurements suggest that there is a critical point quantified by a ρ_{eff} value of 1.20–1.40 g/cm^3 during the transformation of morphology [17, 24, 62]. Besides, the combustion condition is the most crucial in determining the ρ_{eff} value for externally mixed particles. For a homogeneous combustion of diesel fuel in the temperature range of 1400–2200 K, lower-temperature combustion (< 1700 K) produces soot particles with a high organic content and a near-spherical shape. Higher-temperature combustion (> 1900 K) yields particles having fractal morphology [59].

Measurements of BC Optical Properties

Light extinction and absorption of BC containing particles exhibit distinct differences with the morphological change from highly fractal to fully compact during the aging processes. Three general optical parameters used to describe the light extinction capacity with various wavelengths include mass absorption coefficients (MAC), single-scattering albedo (ω_0), and absorption Ångstrom exponent (AAE). Measurements of these values are needed at all wavelengths for optical transfer models to estimate the climate effects of BC [64]. Table 3 summarizes the values of the three optical parameters in recent literature, and the details are discussed in the following subsections.

Mass Absorption Coefficients

Values of MAC (m^2/g) are fundamental inputs to radiative transfer models, required for all aerosols or aerosol components, and are estimated by

$$MAC = \frac{k_{abs}}{m_{conc}} \quad (9)$$

where k_{abs} represent the light-absorption coefficient (m^{-1}) and m_{conc} is the mass concentration (g/m^3) of aerosols. For BC-containing particles, MAC_{BC}, m_{conc} is the BC mass concentration [5]. These quantities are necessary to translate mass concentrations simulated by chemical transport models to their effects on radiative transfer. Since chemical transport models and measurement results often provide BC mass concentrations, the term "MAC" for BC-containing particles often refers to MAC_{BC} without special indication.

Table 2 ρ_{eff} of BC-containing particles in literature

Stages	Emission source	ρ_{eff} (g/cm^3)	D_{mob} (nm)	Refs
Externally mixed	Flame soot	0.10–0.56	126–50 nm	Zhang et al. [2]
		0.10–0.60	350–50 nm	Xue et al. [46]
		0.18–0.41	300–75 nm	Rissler et al. [49]
		0.40–0.55	150–80 nm	Qiu et al. [54]
		0.40–0.80	150–50 nm	Khalizov et al. [48]
		0.18–0.86	637–95 nm	Tavakoli et al. [61]
		0.25–0.46	200–100 nm	Peng et al. [24]
	Diesel exhaust	0.30–0.82	350–50 nm	Rissler et al. [49]
		0.42–0.90	150–50 nm	Barone et al. [57]
		0.26–0.94	400–50 nm	Rissler et al. [60]
		0.09–0.90	707–81 nm	Qiu et al. [59]
	Wood burning	0.25–1.00	400–50 nm	Leskinen et al. [58]
	Urban environments	0.10–0.70	414–322 nm	Geller et al. [56]
		0.51–0.91	230–50 nm	Ma et al. [63]
Internally mixed	Flame soot	0.40–1.60	200–50 nm	Zhang et al. [2]
		0.60–1.10	220–50 nm	Xue et al. [46]
		0.50–1.34	150–80 nm	Qiu et al. [54]
		0.70–1.40	150–50 nm	Khalizov et al. [48]
		0.50–1.40	200–100 nm	Peng et al. [24]
	Diesel exhaust	0.49–1.20	NA	Liu et al. [17]
		0.77–1.97	300–125 nm	Han et al. [53]
	Wood burning	0.40–1.30	400–50 nm	Leskinen et al. [58]
	Urban environments	1.20–1.50	202–50 nm	Geller et al. [56]
		1.40–1.80	240 nm	Liu et al. [62]
		1.30–1.63	230–50 nm	Ma et al. [63]

Table 3 Optical properties of BC-containing particles in literatures

Stages	Optical parameters	Value	Refs
Externally mixed	MAC (m^2/g)	7.50	Bond et al. [1]
		8.28	Zangmeister et al. [66]
	AAE (/)	1.00	Moosmüller et al. [75]
		1.10	Schnaiter et al. [14]
		0.80	Lack and Cappa [83]
		1.05	Liu et al. [74]
	ω_0 (/)	0.10–0.28	Bond et al. [1]
		0.30–0.50	Qiu et al. [59]
		0.20–0.37	Khalizov et al. [88]
		0.38	Bahadur et al. [89]
Internally mixed	AAE (/)	0.80	Schnaiter et al. [14]
		1.90	Lack and Cappa [83]
		0.90	Liu et al. [74]
	ω_0 (/)	0.90	Khalizov et al. [86]
		0.75–0.90	Khalizov et al. [88]

Both laboratory and field-based observations have focused on the measurement of MAC for BC-containing particles. Most studies focus on the wavelength of nearby 550 nm. The most comprehensive assessments of highly absorbing carbonaceous aerosols are reviews by Bond and Bergstrom (2006) which reports a BC MAC ranging from 1.6 to 15.9 m^2/g with an average of 7.5 ± 1.2 m^2/g at $\lambda = 550$ nm for fresh externally mixed BC particles [1], also consistent with measurement results of Clarke et al. [65]. Zangmeister et al. [66] have collected 199 measured values of MAC from published data (1971–2018) for materials reported as BC, which are used to compare with their results highlighting MAC variability due to chemical and physical properties. The results show that MAC at $\lambda = 550$ nm is 8.28 ± 0.34 m^2/g for fresh externally mixed BC particles, 10% higher than the assessment of BC MAC reported by Bond and Bergstrom (2006) [1]. BC particles generated from diesel engines represent the largest single source of reported 199 MAC data (19 reported MAC values). The reported range from diesel exhaust for 514 nm $\leq \lambda \leq$ 532 nm (7 samples) is 7.4 ± 0.5 to 17 m^2/g (no reported uncertainty) with an average of 9.5 ± 3.3 m^2/g. Therein, the error caused by measurement technology including filter or non-filter cannot be ignored. For example, using only data from filter-based studies results in MAC = 9.67 ± 1.50 m^2/g, whereas using photoacoustic spectroscopy data yields MAC = 8.03 ± 0.31 m^2/g. It should be noted that the values listed above are for externally mixed BC particles. Field-based measurements under ambient conditions which include both externally mixed and aged BC report MAC values ranging from 3.8 to 58 m^2/g [67–69]. The BC MAC amplification due to the internally mixing process will be discussed in "Absorption Enhancements".

Absorption Ångstrom Exponent

The wavelength dependence of MAC must be represented in models for the full solar spectrum. The quantity generally used to characterize wavelength variation in absorption is the absorption Ångstrom exponent. Because aerosol absorption normally decreases exponentially with wavelength over the visible and near-infrared spectral region [70–72], the AAE is defined as

$$\mathrm{MAC}(\lambda) = \mathrm{MAC}(\lambda_0)\left(\frac{\lambda}{\lambda_0}\right)^{-\mathrm{AAE}} \quad \text{or} \quad \ln(\mathrm{MAC}(\lambda)) = \ln\left(\mathrm{MAC}(\lambda_0)\right) - \mathrm{AAE} \times \ln\left(\frac{\lambda}{\lambda_0}\right) \tag{10}$$

where $\mathrm{MAC}(\lambda)$ and $\mathrm{MAC}(\lambda_0)$ denote mass absorption cross sections at an arbitrary wavelength λ and a reference wavelength λ_0, respectively. Due to the variation in different ranges of wavelengths, the AAE approximated by Eq. (10) becomes quite sensitive to the choice of observational wavelengths [73]. Two wavelengths spanning the visible range are commonly used, that is, 450 and 650 nm [5]. Since absorption coefficients are proportional to mass absorption cross sections, some studies use absorption coefficients in Eq. (10) [74].

When the size of BC particles is much smaller than the incident light wavelength and the refractive index (usually at visible and near-infrared wavelengths) is wavelength-independent, the Rayleigh approximation theoretically derives an AAE of 1.0 [75], whereas organic aerosols and dust have higher AAE values [76, 77]. Therefore, AAE has been widely used for aerosol characterization studies [77, 78]. The AAE value of an aerosol sample close to 1.0 is considered to be BC-rich aerosol from fossil fuel burning, and larger AAE values are understood to indicate aerosols from biomass/biofuel burning or dust [78]. In another use, AAE has also been quantitatively used to separate brown carbon (BrC) absorption from BC absorption [79, 80]. In the studies of BC/BrC absorption separation, the BrC absorption from biomass burning aerosols is usually retrieved by assuming that BrC contributes no absorption at near-infrared wavelengths and that BC has an AAE of 1.0 [79–81].

However, owing to the intricate emission sources of BC particles, numerous studies have experimentally investigated the value of AAE by measuring the absorption of BC particles [14, 74, 82, 83]. In a laboratory study, Schnaiter et al. (2003) found diesel soot to have an AAE of 1.1 and spark-generated carbon nanoparticles to have an AAE of 2.1 [82]. The different AAE values are mainly attributed to differences in the wavelength dependence of the refractive index for the two emission sources. Day et al. (2006) measured the aerosol light absorptions of fresh wood smoke aerosol between $370 < \lambda < 950$ nm and reported AAE values between 0.9 and 2.2 that strongly depended on the type of wood and burning conditions [84]. In the atmosphere, however, BC particles always co-exist with other aerosol particles. Schnaiter et al. (2005) internally mixed BC particles with secondary organic aerosol in a lab and have found that the coating increases particle sizes [14]. After measuring the absorption of coated BC particles at 450, 550, and 700 nm (see figure 9 of their paper), it is found that coating decreases BC AAE (from approximately 1.1 to 0.8). In contrast, Lack and Cappa (2010) demonstrate that BC AAE increases from 0.8 to 1.9 after coating [83]. In their study, a simplification that coating volume fraction is considered to be equivalent for all particles may be problematic and thereby contradict the measurements by Schnaiter et al. (2005). Liu et al. [74] reached a similar conclusion as Schnaiter et al. (2005) by a numerical study considering multiple controllable variables (such as BC coatings size distribution) that all affect BC AAE. Specifically, the result shows typical BC AAE values of 1.05 and 0.90 for externally and internally mixed BC particles, respectively.

Single-Scattering Albedo

The single-scattering albedo (ω_0) is scattering divided by extinction (i.e., the sum of scattering and absorption), which represents the aerosol properties most relevant to the balance between negative and positive radiative forcing. Values of ω_0 near 1 indicate that the aerosol is mainly scattering, and only for values below about 0.8 could the particles exert a net warming effect in the atmosphere for clear-sky conditions [85].

For BC particles, the ω_0 value of freshly generated aggregates has been measured as 0.10 to 0.28 [1]. As BC becomes internally mixed with other aerosol components, the value ranges from that of fresh particles to 0.9 depending upon the amount of coating material [86, 87]. Besides, combustion temperatures are considered to be essential impactors of the ω_0 value [59, 88]. Their studies show that combustion of the leaner propane/oxygen mixtures produces BC particles with ω_0 in the range of 0.3–0.5, without notable temperature dependence. On the contrary, ω_0 of BC produced using the more fuel-rich mixtures shows a strong dependence on the combustion temperature. For all of the fuel equivalence ratios tested in their studies, ω_0 is relatively high (0.75/0.90) for BC produced at a lower combustion temperature (1796/1400 K) but decreases to values as low as 0.37/0.20 when the combustion temperature exceeds 1876/2100 K. The major cause for the temperature dependence is probably the composition and morphology variation due to the temperature condition, as mentioned in the section of Effective Density.

The spectral dependence of ω_0 has also been proved by the ground-based Aerosol Robotic Network (AERONET), a globally distributed network of automated sun and sky radiometers, which provides long-term, continuous, and readily available measurements of aerosol optical properties [89]. The association is proved to be weak, and the ω_0 value of 0.38 at 870 nm is recommended, which is higher than that typically reported by Bond and Bergstrom (2006) [1].

Absorption Enhancement

Internal mixing between BC and scattering coatings increases light absorption of visible bands, in part because the non-absorbing material can refract light toward the absorbing particle known as "lensing effect" [90]. Light absorption enhancement (E_{abs}) due to lensing has been observed for BC particles coated with SOA [14] or sulfuric acid [2], for graphite coated with oleic acid or glycerol [91], for absorbing biomass-burning emitted particles coated with organic material [16], and for absorbing fuel combustion BC internally mixed with ammonium sulfate or sodium chloride [91]. E_{abs} caused by a mixing state is defined as the ratio of internally mixed MAC to that of an external mixing state with equivalent BC mass. Values of E_{abs} have been widely observed across the visible radiation spectrum represented by wavelengths of 405 nm and 532 nm using filter or photoacoustic methods, which require measuring MAC before and after removal of coatings with thermal or laser-induced methods [5, 92–94]. Throughout laboratory measurements, controlled experimental conditions provide quantified impacts of the mixing state on E_{abs}, whereas field-based observations concentrate on the spatial and temporal distribution of E_{abs} values. A recent report using such a heating denuder method suggests negligible absorption enhancement of BC in ambient aerosols in North America [15], which contracts to theoretical estimations of a factor ~ 2 [9]. Therefore, due to various experimental conditions, there is an intense debate about the issue of absorption enhancement.

As depicted by previous observations, the degree to which BC particles absorb light depends on their coating components influenced by emission source and mixing state depicted with parameters in "Fractal Dimension." By sorting the E_{abs} values published in the literature since 2005, Fig. 3 demonstrates that previous laboratory studies [2, 14, 16, 22, 24, 86, 91, 95, 96] yielded a broad range of MAC enhancements from 1.9–2.5 and 1.31–3.5 at wavelengths of 405 nm and 532 nm, varying with the mass ratio of non-BC matter to BC (M_R). On the contrary, a field measurement indicates slightly lower values than laboratory results that range from 1.13–3.5 and 1.06–2.7 at wavelengths of 405 nm and 532 nm [15, 17, 23, 28, 97–100]. In particular, the mild larger E_{abs} values at 405 nm for the same literature (as shown in Fig. 3a) with identical mixtures likely indicates the influence of coating absorption in this wavelength region. It is generally known that purely scattering materials coated on BC particles can significantly enhance absorption due to the focus light toward the BC core. However, if coating components become absorptive materials (i.e., brown carbon) the values of E_{abs} will be increased as a result of absorbing radiation by non-BC materials. Field measurements equipped with SP-AMS can exclusively characterize the size distributions as well as chemical compositions of BC cores and the coating materials, and their results indicate that brown carbon contributed to the observed E_{abs} at 405 nm [92, 93]. In addition to the optical properties of coating components, the evolution of E_{abs} exhibits two distinct stages (Fig. 3b). At the initial stage of BC coating with M_R less than ~ 3, BC absorption enhancement is limited to less than 5% [15, 88]. Cappa et al. (2012) hypothesized that the low values of enhancement are caused by BC inclusions at the edge of the sampled particles [15]. When M_R is between ~ 5 and ~ 200, E_{abs} rapidly rises with the augment of the non-BC mass. The averaged E_{abs} seems to become stable to be ~ 2.1–2.6 for $M_R \geq 50$ [24, 100]. The lab-measured E_{abs} floating up to 3.5 is a notable value which condenses hydrophilic materials (i.e., glutaric acid vapor) into fresh BC aerosols and then investigates BC-water drop mixtures at relative humidity increasing up to 100% [22].

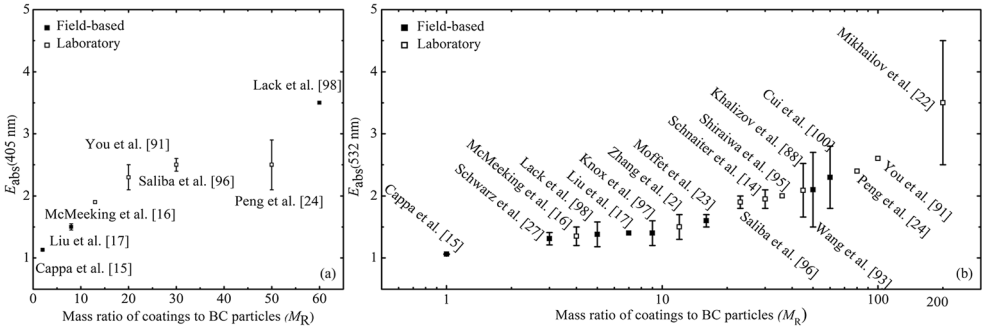

Fig. 3 Light absorption enhancement (E_{abs}) at wavelengths of 405 nm and 532 nm of previously published data. The error bars represent 2σ uncertainty

Consequently, coatings affect light absorption enhancement through at least three mechanisms: (a) non-absorbing coatings can direct more light to BC particles than it would otherwise receive ("lensing effect"), enhancing the total absorption; (b) the coating can absorb light directly if it has a nonzero imaginary refractive index which leads to more enhancement than mere lensing effect; and (c) the addition of coatings can cause fractal BC morphologies to collapse to more compact, spherical shapes, which can reduce the amount of light absorbed, probably resulting in the lower values with the initial transformation from a fractal to spherical morphology. In this second case, measured E_{abs} values affected by coating absorption is inappropriate to represent pure BC light absorption enhancement, which essentially contains light absorption of coatings [83, 98]. MAC of brown carbon has been estimated to be of the same order as BC at 400 nm [101, 102], and a large amount of directly emitted organic matters (i.e., brown carbon) is internally mixed with BC from sources such as biomass and biofuel combustion [103, 104]. It is, therefore reasonable to explain that E_{abs} values at 532 nm are more representative than those at 405 nm for BC absorption enhancements caused by internal mixing, especially when the emission source is biomass burning dominated.

Modeling of the BC Mixing State and Optical Properties

To determine the macroscopic absorption and scattering of BC-containing particles, the physicochemical properties of individual species are required that can serve as inputs, such as particle size, morphology, and refractive index [6]. Therefore, optical properties of BC-containing particles are closely tied to the mixing state [105]. Concurrent with advances in modeling methods, modeling tools have become sufficiently complex to incorporate aspects of the mixing state in their applications. In this section, we will first review the BC mixing state in different aerosol models, and then describe existing optical modeling approaches.

Mixing State Representation in Models

It is common to use a continuous number distribution as a function of particle size that predicts its evolution in aerosol science. However, it is important to realize that in doing so, the high-dimensional composition space is projected onto one dimension (size), thereby losing information about per-particle composition. Therefore, a generalized number distribution with respect to aerosol species is introduced to resolve the mixing state [106]. The cumulative aerosol number distribution at constituent masses $\overrightarrow{\mu}\epsilon\mathbb{R}^A$, time t, and location $\overrightarrow{x}$ is $\mathrm{N}\left(\overrightarrow{\mu}, t, \overrightarrow{x}\right)$ (m^{-3}), then the number distribution is defined by

$$\mathrm{n}\left(\overrightarrow{\mu}, t, \overrightarrow{x}\right) = \frac{\partial^A N\left(\overrightarrow{\mu}, t, \overrightarrow{x}\right)}{\partial\mu_1\partial\mu_2\cdots\partial\mu_A} \tag{11}$$

where the A-dimensional vector $\overrightarrow{\mu}$ is used to denote aerosol particles that contain less than μ_α mass of species α, for all $\alpha = 1,\ldots, A$. The classical Smoluchowski coagulation equation [107, 108] provides a solution for the multidimensional aerosol number distribution in Eq. (11), and has been previously described in detail by Riemer et al. [106, 109].

Mixing states in aerosol models are characterized by the way they discretize the aerosol number distribution function, $n\left(\overrightarrow{\mu}, t, \overrightarrow{x}\right)$. According to the method of discretization, the main categories of modeling approaches include bulk models, modal models, moment models, sectional models, and particle-resolved models. In this section, we present how these approaches handle the representation of the BC mixing state.

Limited by computational resources, BC particles are treated as externally mixed with other aerosol species (e.g., sulfate, organic carbon, sea salt, and dust) for bulk models [110, 111]. To better simulate the atmospheric aging, the transformation of fresh to aged BC particles is often treated as an exponential decay process with a constant half-life [110, 112]. This approach is computationally efficient, and often used in general circulation models (GCM), such as the Goddard Institute for Space Studies (GISS) GCM and the ECHAM GCM. As mentioned in "Measurement of BC States", BC aging depends on the emission and environmental conditions. The constant

aging half-life for BC particles could introduce significant uncertainties.

For distribution-based models (e.g., modal and sectional models), rules need to be defined to handle the interactions of number distribution functions for BC and mixtures. The underlying assumption of modal models is that they represent BC particle distribution as a sum of modes, and each has a log-normal (or similar) size distribution described by a small number of parameters (typically number, mass, and width). This modeling framework has been adopted in many global and regional models [113–117]. The choice of number of modes has to be made considering which chemical species are present in various modes, and different models differ in their assumptions. Remarkably, one guiding principle has been to keep freshly emitted BC particles separately from mixtures with secondary species. For example, in the Community Multiscale Air Quality Modeling System (CMAQ) model, BC is emitted into Aitken and Accumulation modes, respectively [118]. To set up destination modes to represent coagulation between modes, rules describing mode interactions need to be defined [119], which also vary between different models. Due to the variations including interaction rules and mode numbers, there are inevitable uncertainties in modal models.

While modal models use several overlapping log-normal function within a size range, sectional models place a grid on the independent variable space and store the number distribution in each grid cell. BC mixing states can be solved by introducing several, potentially interacting univariate distributions [120–123]. Three BC-containing distributions with different amounts of non-BC components are used in this approach [120]. Another possibility is to use a two-dimensional sectional framework to represent BC inclusions, with one dimension being dry diameter and the other dimension being mass fraction. The application includes Weather and Research Forecasting model coupled with Chemistry (WRF-Chem) [121], mixing-state-resolved sectional aerosol model (MOSAIC-MIX) [123], and Size-Composition Resolved Aerosol Model (SCRAM) [122]. This approach is computationally more expensive than the modal modeling approach, because more variables are tracked for each distribution.

Moment models do not explicitly resolve the distribution, but rather track the lower-order moments of it. Closure of the moment evolution equations is the key issue for this approach. With the introduction of the quadrature method of moment (QMOM) [124, 125], mixing states can be treated without the need for a priori assumptions about the size distribution. The method has also been used in a bivariate test tracking of BC mixing states and benchmarked with particle-resolved model results [126]. The result shows that low-order quadratures are found to be highly accurate and feasible to represent mixing states in large-scale models. Additionally, simulations of aerosol dynamics based on moments are free from uncertainties associated with particle size space and tend to have greatly superior computational speed when compared with the distribution-based approach.

In contrast to the above approaches, particle-resolved models explicitly resolve high-dimensional composition spaces for BC inclusions and provide a tool for benchmarking aerosol models with respect to mixing states. The method assumes each particle as an A-dimensional vector $\overrightarrow{\mu} \epsilon \mathbb{R}^A$ with components $(\mu_1^i, \mu_2^i, \cdots, \mu_A^i)$, with μ_a^i being the mass of species α in particle i, for $\alpha = 1, \cdots, A$ and $i = 1, \cdots, N_p$. The composition of each particle can change accompanied with condensation and evaporation, and the Monte Carlo approach is also applied for simulating the evolution of particle distributions [106]. For example, a particle-resolved model coupled with Model for Simulating Aerosol Interactions and Chemistry (PartMC-MOSAIC) has been developed by Zaveri et al. [127] and Riemer et al. [106] and applied to simulate the aging process of BC in an evolving aerosol population. They have found that a continuum of BC mixing states existed after 24 h of simulation in the context of an idealized example of an urban plume case. It is worth pointing out that the information about morphology, fractal dimension, and the internal structure of the particles is not tracked even in particle-resolved models. This information plays a key role in the calculation of optical properties which will be discussed in the next section.

Optical Models

Approximate models such as the core-shell model or equivalent homogeneous approximations ignore the chain-like aggregate structure and overestimate the light absorption of BC [17]. The optical properties of aggregates considering the mixing state of different components have been extensively studied numerically in the past two decades [32, 74, 128, 129]. The numerical solutions can be classified into approximate and sophisticated methods according to the theory of computation, and they can provide BC optical properties with different computational accuracies and efficiencies [130]. Due to the observed high complexity and large variations in BC structures, most current experiments or field campaigns cannot provide sufficient observational results for the sophisticated modeling studies [131–133]. How to choose an appropriate numerical scheme for various observation results becomes one of the most fundamental and important methods to improve our understanding of the effects of coating on BC optical properties. The general connections between mixing properties and modeling the optical properties of BC-containing particles are shown in Fig. 4.

Figure 4 summarizes particle properties constrained by measurements and optical theories to adapt to the mixing

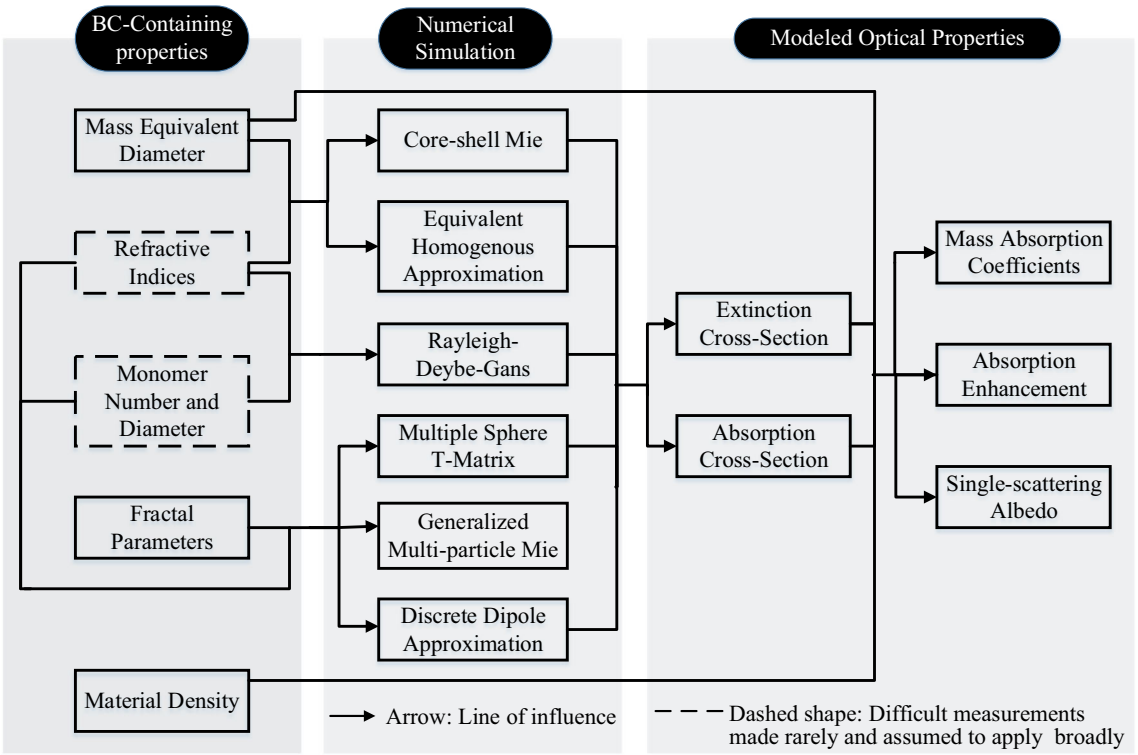

Fig. 4 Schematic of the connections between the properties of BC-containing particles and modeled optical properties

configuration. Refractive indices of the bulk material are required to calculate MAC for all models, whereas parameters used to depict shape and size become not uniform for distinct models. Global-model calculations of radiative transfer usually use Mie theory with the core–shell assumption or dielectric mixing rule for homogeneous mixing [43, 134, 135]. However, even with relatively small particle sizes, optical properties of the highly complex aggregates cannot be represented by those of spheres with equivalent mass. To account for the fractal nature of BC particles, common optical-modeling treatments include the Rayleigh–Debye–Gans (RDG) approximation [136], multiple-sphere T-matrix (MSTM) theory [129, 137], generalized multi-particle Mie (GMM) method [138–140], and discrete dipole approximation (DDA) method [141, 142]. The theory of optical models and required inputs is essential to explaining model errors; a detailed discussion is then subsequently revealed.

The core–shell Mie model assumes that both the BC core and outer shell are homogeneous (Fig. 5a) and then require several input parameters, e.g., the sizes of the inner BC core and outer shell, the refractive indices of the BC core, and coating materials at interested wavelengths. For the equivalent diameter discussed in "Equivalent Diameters," the core of internally mixed BC particles is appropriate to be represented

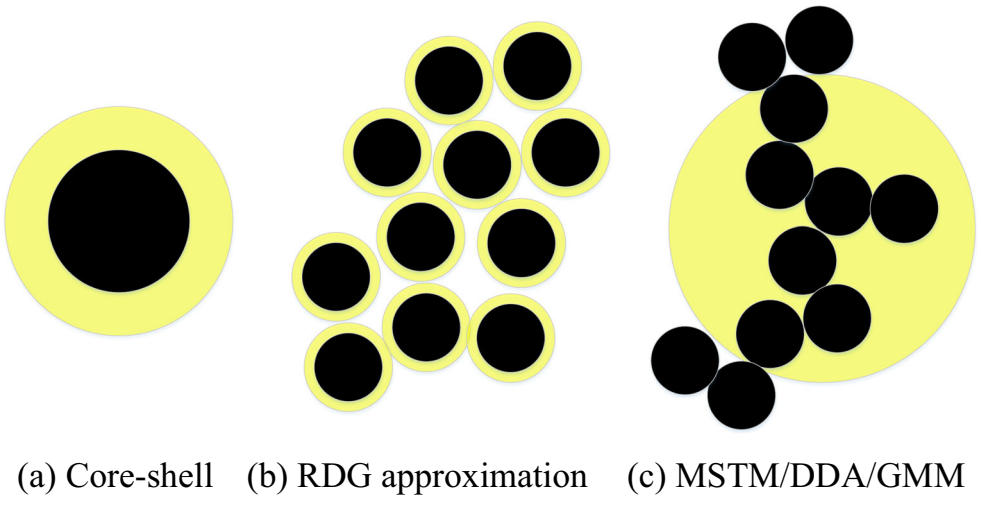

Fig. 5 A schematic of the models used to estimate the optical properties of the BC-containing particles. **a** Core–shell. **b** RDG approximation. **c** MSTM/DDA/GMM

as the mass equivalent diameter (D_{me}) of fresh BC particles [17, 24, 143]. The other two equivalent diameter D_{mob} and D_a need to be transformed into D_{me} through approximate relation.

Based on the Mie theory, the above core–shell assumption for solving the macroscopic Maxwell equations with a multi-layered sphere [144] is taken into account when modeling the radiation of BC-containing particles; instead, the effective medium approximation methods (i.e., Bruggeman mixing rule or Maxwell–Garnett mixing rule) hypothesize the composite materials as a homogenous mixing sphere (or called effective medium) that has an effective refractive index (m) calculated by Eqs. (12)–(14).

$$m = \sqrt{\epsilon} \tag{12}$$

where ϵ denotes the effective dielectric constant. The Bruggeman mixing rule [145] treats all materials on an equal base with the mixture of different components attached. The Bruggeman mixing rule is given by

$$V_1 \frac{\epsilon_1 - \epsilon}{\epsilon_1 + 2\epsilon} + V_2 \frac{\epsilon_2 - \epsilon}{\epsilon_2 + 2\epsilon} + V_3 \frac{\epsilon_3 - \epsilon}{\epsilon_3 + 2\epsilon} + \ldots = 0, \quad (V_1 + V_2 + V_3 + \ldots = 1) \tag{13}$$

where all ϵ_n ($n = 1, 2, 3, ...$) refer to the dielectric constant of individual components and V_n ($n = 1, 2, 3, ...$) is the volume fraction of the dielectric component and absorbing components. The Maxwell–Garnett mixing rule [146] assumes that a host material contains all other composite materials. The Maxwell–Garnett mixing rule is given by

$$\frac{\epsilon - \epsilon_1}{\epsilon + 2\epsilon_1} = V_2 \frac{\epsilon_2 - \epsilon_1}{\epsilon_2 + 2\epsilon_1} + V_3 \frac{\epsilon_3 - \epsilon_1}{\epsilon_3 + 2\epsilon_1} + \ldots, (V_1 + V_2 + V_3 + \ldots = 1) \tag{14}$$

where ϵ is the effective dielectric constant and ϵ_1 is the dielectric constant of the host material which contains all other composite materials. More details on the difference of effective medium approximation methods can be found in the algorithms comparison given by Liu [147].

With the assumption of no internal multiple scattering among BC monomers (Fig. 5b), the so-called Rayleigh–Debye–Gans (RDG) approximation [32] used to estimate the absorption cross section (σ_{abs}) of the aggregate can be obtained by

$$\sigma_{abs} = N(\pi a^2) Q_{abs} = N(\pi a^2) 4 \frac{2\pi a}{\lambda} Im\left\{\frac{m^2 - 1}{m^2 + 2}\right\} \tag{15}$$

where N and a are similar to Eq. (1), Q_{abs} is the absorption efficiency of the spherule at the radiation wavelength of λ, and m is similar to Eq. (12).

Among all the estimated properties shown in the right portion of Fig. 4, extinction and absorption cross sections (σ_{ext} and σ_{abs}) are the direct output of the above models, and the other parameters are usually calculated to compare with measurements. The mass absorption coefficient (MAC) is calculated by

$$MAC = \frac{\sigma_{abs}}{M_{BC}} \tag{16}$$

where M_{BC} is similar to Eq. (5) influenced by BC diameter and density. Compared with Eq. (9), it is noted that the calculation of MAC is different between the simulation and observation owing to the distinction of directly obtained parameters. Subsequently, E_{abs} can be predicted according to externally and internally mixed MAC, with the same definition of measurements mentioned in "Mass Absorption Coefficients" and "Absorption Ångstrom Exponent."

Beyond the approximate methods mentioned above, sophisticated methods (e.g., MSTM, GMM, DDA) are much more time-consuming but closer to reality with precisely defined geometry [130, 133, 148]. The modeled MAC for external mixing states ranges from 5.53 to 6.79 m^2/g at a wavelength of 550 nm, as shown in Fig. 6 [43, 96, 128, 131, 149–159], which is smaller than the measured values 7.5 ± 1.2 m^2/g [1] and 8.28 ± 0.34 m^2/g [66]. The discrepancy between measured and modeled values is dominated by the refractive indices and fractal parameters listed in the left portion of Fig. 4 [150, 159]. We can also obtain that DDA and MSTM calculated a 10 to 20% increase for many changes in fractal parameters, compared with the RDG approximation neglecting electromagnetic interactions among monomers. To account for the optical properties of randomly oriented particles, DDA has to be applied multiple times for averaging over different particle orientations, whereas only one simulation is needed for the MSTM. The GMM code is serial, and its computational time is divided by the number of processes used by the other models for fair comparison. For computational efficiency, the MSTM is the most efficient one, which is approximately one and two orders of magnitude faster than the GMM and DDA, respectively [131]. Because these sophisticated methods are based on a precise aggregate structure, a flexible tunable aggregation algorithm [160] with fractal parameters as inputs becomes necessary for these three methods, which can generate BC aggregative morphology (Fig. 5c). Besides, the DDA method is based on solving Maxwell's equations in the frequency domain of arbitrary particle shape and can be extended to quantify the effects of minor imperfect structures (e.g., irregularity and coating of individual BC monomer) on optical properties [161].

In particular, there are inevitable errors among the aforementioned models within various inputs. When the core–shell Mie theory is applied to aerosol models, the coating fraction determined by aerosol models becomes an important influence factor. Jacobson (2010) has proved that the value of

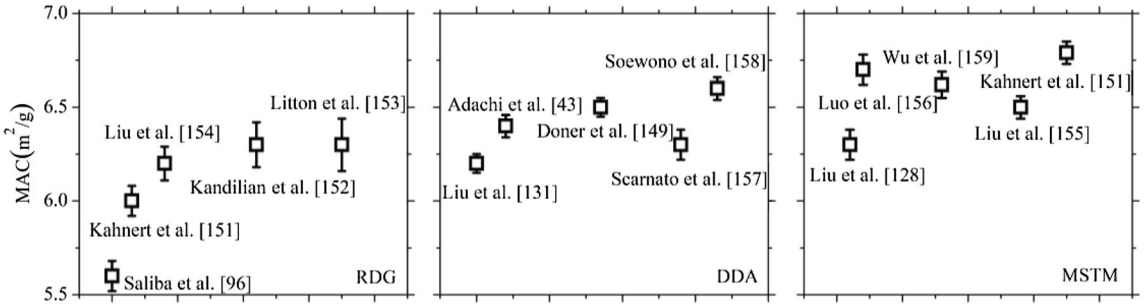

Fig. 6 Modeled MAC of externally mixed BC particles at wavelength of 550 nm. The error bars represent 2σ uncertainty

E_{abs} offers a range of 2~3 depending on the coating fraction that is simulated by a sectional modal with 14 size bins [162]. Another explanation was put forward by Fierce et al. (2016) who used PartMC-MOSAIC to evaluate the coating distributions (Fierce et al., 2016). They found that assuming the mass fractions of coatings and cores as a constant across all core sizes led to a two-fold overestimation of absorption enhancement. Furthermore, the refractive index of coating materials is critical in determining whether the substance is non-absorbable and therefore affects the estimated optical properties of internally mixed BC particles. Black carbon and organic matters have imaginary parts on the order of 10^{-1} and 10^{-2}, while water and sulfate are almost non-absorbing with values from less than 10^{-6} at visible wavelengths to approximately 10^{-3} at near-infrared wavelengths [6, 163]. As the coating component changes from sulfate to organic matter, the absorption section of the core–shell model increases by 30 to 40%, but up to a 20% decrease for ω_o with relative humidity larger than 90% [19]. The conclusion based on simulation keeps consistent with the measured E_{abs} depicted in "Absorption Ångstrom Exponent." The mixing rule method is useful for exploring how the coating fraction affects the internally mixed refractive index. With the increase in coating fraction, the mixed refractive index becomes closer to the value of non-BC material, and hence a large increase in ω_o floating up to 0.8~0.9 [164, 165].

The D_f value plays the most essential role in the aggregation simulation of externally mixed optical properties. Size-averaged results demonstrate that freshly emitted BC particles tend to absorb more light with an increase in D_f and predict ω_o decrease from 0.3 to 0.1 [128]. This may be the consequence of the shielding effect of the outer layer of monomers that blocks light from penetrating deeply inside a compact aggregate. When BC-containing particles transform into internally mixed, the relative position between BC aggregates and coating materials becomes a particularly important model input [131, 132]. BC-containing particles with partially encapsulated mixing states yield a value of E_{abs} less than 2, yet the value can float up to 3.5 under a fully coated assumption with the value of D_f increasing to 2.8 [132].

In general, it is essential to apply appropriate inputs for models to improve modeling accuracy. Recent studies under ambient conditions show that it exhibits a multistage process from external to internal mixing states, and the core–shell model tends to overestimate the absorption at the initial process; besides, it predicts a reasonable range for fully coated BC [17, 24]. By comparing the core–shell method with ambient measurements, Liu et al. (2017) found that the core–shell model becomes closer to measurements when M_R is above the transition threshold of BC aging [17]. To compare MSTM with ambient measurements, Wu et al. (2018) show that the model predictions of M_R-dependent optical properties are improved by integrating BC realistic morphological inputs of mixing states, leading to the decline in simulation errors of MAC from ~ 20.6 to ~ 5.1% on average [132]. Therefore, it is necessary to apply correction coefficients to the widely used core–shell assumption for adjusting the uncertainty of optical properties.

Summary and Conclusions

This paper reviews progress in recent studies related to mixing states and influence on the optical properties of BC. Fractal dimension, equivalent diameter, and effective density (ρ_{eff}) are used to characterize BC morphology, and these parameters are influenced by mixing states and emission sources. The transformation of mixing states from a highly fractal nature to a more compact sphere can be reflected by measuring the decreased electric mobility diameter at the same mass, but increase in fractal dimension and effective density. Studies show that fractal dimension increases from 1.53–1.83 to 1.86–2.16 after BC being internally mixed with other aerosols. The transition in ρ_{eff} has been reported in literatures occurring at 1.20–1.40 g/cm^3. Traffic BC-containing particles have a more spherical shape than wildfire emissions during atmospheric aging because former mixtures have higher levels of condensable materials with higher hygroscopicity.

Besides mixing states and emission profiles, the spectral dependence of radiative properties (i.e., MAC, AAE, ω_0, and E_{abs}) must also be considered. Because MAC of brown carbon has the same order as that of black carbon at 400 nm, E_{abs} values at 532 nm are more representative than those at 405 nm for absorption enhancements of black carbon. Moreover, there

are large variations in measured E_{abs} for both laboratory and field measurements. Published E_{abs} at a wavelength of 532 nm varied from 1.06 to 2.7 and 1.31 to 3.5 for laboratory and field measurements, respectively.

Both aerosol models and optical approaches have been developed to improve our understanding on BC optical properties influenced by mixing states. Due to the evitable algorithm errors introduced by approximate methods, sophisticated methods, and aggregation structure, attempts have been made to provide benchmark approaches for the simulation of optical properties. As we have discussed in this paper, particle-resolved aerosol models are suitable for explicitly resolving high-dimensional composition spaces that are common for BC-containing particles. With the development of aerosol models and optical approaches, high-dimensional composition spaces for BC inclusions can be solved by particle-resolved models, and optical properties of particles with arbitrary shape or anisotropic composition have also been calculated by sophisticated approaches. However, such models are much more complex and time-consuming and lacks shape information in aerosol models. In order to establish accurate modeling methods, more efforts should be devoted to the collaboration of aerosol models and optical approaches and to the development of chemical transport models that can reliably predict aerosol optical properties based on the evolution of the physicochemical mixing state coupled with sophisticated optical models.

Funding Information This work was supported by the National Key R&D Program of China (2018YFC0213800), the National Natural Science Foundation of China (41975162, 21777073, and 41675125), and an open fund by Jiangsu Key Laboratory of Atmospheric Environment Monitoring and Pollution Control (KHK1908).

Compliance with Ethical Standards

Conflict of Interest On behalf of all authors, the corresponding author states that there is no conflict of interest.

Human and Animal Rights and Informed Consent This article does not contain any studies with human or animal subjects performed by any of the authors.

References

1. Bond TC, Bergstrom RW. Light absorption by carbonaceous particles: an investigative review. Aerosol Sci Technol. 2006;40(1):27–67. https://doi.org/10.1080/02786820500421521.
2. Zhang R, Khalizov AF, Pagels J, Zhang D, Xue H, McMurry PH. Variability in morphology, hygroscopicity, and optical properties of soot aerosols during atmospheric processing. Proc Natl Acad Sci. 2008;105(30):10291–6. https://doi.org/10.1073/pnas.0804860105.
3. Schwarz JP, Spackman JR, Gao RS, Watts LA, Stier P, Schulz M, et al. Global-scale black carbon profiles observed in the remote atmosphere and compared to models. Geophys Res Lett. 2010;37(18). https://doi.org/10.1029/2010gl044372.
4. Han C, Liu Y, Ma J, He H. Effect of soot microstructure on its ozonization reactivity. J Chem Phys. 2012;137:084507. https://doi.org/10.1063/1.4747190.
5. Bond TC, Doherty SJ, Fahey DW, Forster PM, Berntsen T, DeAngelo BJ, et al. Bounding the role of black carbon in the climate system: a scientific assessment. J Geophys Res-Atmos. 2013;118(11):5380–552. https://doi.org/10.1002/jgrd.50171.
6. Hess M, Koepke P, Schult I. Optical properties of aerosols and clouds: the software package OPAC. Bull Am Meteorol Soc. 1998;79:831–44. https://doi.org/10.1175/1520-0477(1998)079<0831:OPOAAC>2.0.CO;2.
7. Ogren JA, Charlson RJ. Elemental carbon in the atmosphere: cycle and lifetime. Tellus Ser B Chem Phys Meteorol. 1983;35(4):241–54. https://doi.org/10.3402/tellusb.v35i4.14612.
8. Stier P, Seinfeld JH, Kinne S, Boucher O. Aerosol absorption and radiative forcing. Atmos Chem Phys. 2007;7(19):5237–61. https://doi.org/10.5194/acp-7-5237-2007.
9. Jacobson MZ. Strong radiative heating due to the mixing state of black carbon in atmospheric aerosols. Nature. 2001;409(6821):695–7. https://doi.org/10.1038/35055518.
10. Ramanathan V, Carmichael G. Global and regional climate changes due to black carbon. Nat Geosci. 2008;1(4):221–7. https://doi.org/10.1038/ngeo156.
11. Li J, Pósfai M, Hobbs PV, Buseck PR. Individual aerosol particles from biomass burning in southern Africa: 2, Compositions and aging of inorganic particles. J Geophys Res-Atmos. 2003;108(D13). https://doi.org/10.1029/2002jd002310.
12. Mallet M, Roger JC, Despiau S, Putaud JP, Dubovik O. A study of the mixing state of black carbon in urban zone. J Geophys Res-Atmos. 2004;109(D4). https://doi.org/10.1029/2003jd003940.
13. China S, Mazzoleni C, Gorkowski K, Aiken AC, Dubey MK. Morphology and mixing state of individual freshly emitted wildfire carbonaceous particles. Nat Commun. 2013;4(1):2122. https://doi.org/10.1038/ncomms3122.
14. Schnaiter M, Linke C, Möhler O, Naumann K-H, Saathoff H, Wagner R, et al. Absorption amplification of black carbon internally mixed with secondary organic aerosol. J Geophys Res-Atmos. 2005;110(D19). https://doi.org/10.1029/2005jd006046.
15. Cappa CD, Onasch TB, Massoli P, Worsnop DR, Bates TS, Cross ES, et al. Radiative absorption enhancements due to the mixing state of atmospheric black carbon. Science. 2012;337(6098):1078–81. https://doi.org/10.1126/science.1223447.
16. McMeeking GR, Fortner E, Onasch TB, Taylor JW, Flynn M, Coe H, et al. Impacts of nonrefractory material on light absorption by aerosols emitted from biomass burning. J Geophys Res-Atmos. 2014;119(21):12,272–12,86. https://doi.org/10.1002/2014jd021750.
17. Liu D, Whitehead J, Alfarra MR, Reyes-Villegas E, Spracklen Dominick V, Reddington Carly L, et al. Black-carbon absorption enhancement in the atmosphere determined by particle mixing state. Nat Geosci. 2017;10(3):184–8. https://doi.org/10.1038/ngeo2901.
18. Liu L, Mishchenko M. Scattering and radiative properties of morphologically complex carbonaceous aerosols: a systematic modeling study. Remote Sens. 2018;10:1634. https://doi.org/10.3390/rs10101634.
19. Zeng C, Liu C, Li J, Zhu B, Yin Y, Wang Y. Optical properties and radiative forcing of aged BC due to hygroscopic growth: effects of the aggregate structure. J Geophys Res-Atmos. 2019;124(8):4620–33. https://doi.org/10.1029/2018jd029809.
20. Jacobson MZ. A physically-based treatment of elemental carbon optics: implications for global direct forcing of aerosols. Geophys Res Lett. 2000;27(2):217–20. https://doi.org/10.1029/1999gl010968.

21. Hansen J, Sato M, Ruedy R, Lacis A, Oinas V. Global warming in the twenty-first century: an alternative scenario. Proc Natl Acad Sci. 2000;97(18):9875–80. https://doi.org/10.1073/pnas.170278997.
22. Mikhailov EF, Vlasenko SS, Podgorny IA, Ramanathan V, Corrigan CE. Optical properties of soot–water drop agglomerates: an experimental study. J Geophys Res-Atmos. 2006;111(D7). https://doi.org/10.1029/2005jd006389.
23. Moffet RC, Prather KA. In-situ measurements of the mixing state and optical properties of soot with implications for radiative forcing estimates. Proc Natl Acad Sci. 2009;106(29):11872–7. https://doi.org/10.1073/pnas.0900040106.
24. Peng J, Hu M, Guo S, Du Z, Zheng J, Shang D, et al. Markedly enhanced absorption and direct radiative forcing of black carbon under polluted urban environments. Proc Natl Acad Sci. 2016;113(16):4266–71. https://doi.org/10.1073/pnas.1602310113.
25. Rosen H, Hansen ADA, Gundel L, Novakov T. Identification of the optically absorbing component in urban aerosols. Appl Opt. 1978;17:3859–61. https://doi.org/10.1364/AO.17.003859.
26. Dippel B, Jander H, Heintzenberg J. NIR FT Raman spectroscopic study of flame soot. Phys Chem Chem Phys (Incorporating Faraday Transactions). 1999;1:4707–12. https://doi.org/10.1039/A904529E.
27. Schwarz JP, Gao RS, Fahey DW, Thomson DS, Watts LA, Wilson JC et al. Single-particle measurements of midlatitude black carbon and light-scattering aerosols from the boundary layer to the lower stratosphere. Journal of Geophysical Research: Atmospheres. 2006;111(D16). https://doi.org/10.1029/2006jd007076.
28. Schwarz JP, Spackman JR, Fahey DW, Gao RS, Lohmann U, Stier P, et al. Coatings and their enhancement of black carbon light absorption in the tropical atmosphere. J Geophys Res-Atmos. 2008;113(D3). https://doi.org/10.1029/2007jd009042.
29. Onasch TB, Trimborn A, Fortner EC, Jayne JT, Kok GL, Williams LR, et al. Soot particle aerosol mass spectrometer: development, validation, and initial application. Aerosol Sci Technol. 2012;46(7):804–17. https://doi.org/10.1080/02786826.2012.663948.
30. Moosmüller H, Chakrabarty RK, Arnott WP. Aerosol light absorption and its measurement: a review. J Quant Spectrosc Radiat Transf. 2009;110(11):844–78. https://doi.org/10.1016/j.jqsrt.2009.02.035.
31. Lack DA, Lovejoy ER, Baynard T, Pettersson A, Ravishankara AR. Aerosol absorption measurement using photoacoustic spectroscopy: sensitivity, calibration, and uncertainty developments. Aerosol Sci Technol. 2006;40(9):697–708. https://doi.org/10.1080/02786820600803917.
32. Sorensen CM. Light scattering by fractal aggregates: a review. Aerosol Sci Technol. 2001;35(2):648–87. https://doi.org/10.1080/02786820117868.
33. China S, Salvadori N, Mazzoleni C. Effect of traffic and driving characteristics on morphology of atmospheric soot particles at freeway on-ramps. Environ Sci Technol. 2014;48(6):3128–35. https://doi.org/10.1021/es405178n.
34. Wang Y, Liu F, He C, Bi L, Cheng T, Wang Z, et al. Fractal dimensions and mixing structures of soot particles during atmospheric processing. Environ Sci Technol Lett. 2017;4(11):487–93. https://doi.org/10.1021/acs.estlett.7b00418.
35. Yuan Q, Xu J, Wang Y, Zhang X, Pang Y, Liu L, et al. Mixing state and fractal dimension of soot particles at a remote site in the southeastern Tibetan Plateau. Environ Sci Technol. 2019;53(14):8227–34. https://doi.org/10.1021/acs.est.9b01917.
36. Lee KO, Cole R, Sekar R, Choi MY, Kang JS, Bae CS, et al. Morphological investigation of the microstructure, dimensions, and fractal geometry of diesel particulates. Proc Combust Inst. 2002;29(1):647–53. https://doi.org/10.1016/S1540-7489(02)80083-9.
37. Zhu J, Lee KO, Yozgatligil A, Choi MY. Effects of engine operating conditions on morphology, microstructure, and fractal geometry of light-duty diesel engine particulates. Proc Combust Inst. 2005;30(2):2781–9. https://doi.org/10.1016/j.proci.2004.08.232.
38. Chakrabarty RK, Moosmüller H, Garro MA, Arnott WP, Walker J, Susott RA, et al. Emissions from the laboratory combustion of wildland fuels: particle morphology and size. J Geophys Res-Atmos. 2006;111(D7). https://doi.org/10.1029/2005jd006659.
39. Chandler MF, Teng Y, Koylu UO. Diesel engine particulate emissions: a comparison of mobility and microscopy size measurements. Proc Combust Inst. 2007;31(2):2971–9. https://doi.org/10.1016/j.proci.2006.07.200.
40. Soewono A, Rogak S. Morphology and Raman spectra of engine-emitted particulates. Aerosol Sci Technol. 2011;45(10):1206–16. https://doi.org/10.1080/02786826.2011.587036.
41. Seong HJ, Boehman AL. Evaluation of Raman parameters using visible Raman microscopy for soot oxidative reactivity. Energy Fuel. 2013;27(3):1613–24. https://doi.org/10.1021/ef301520y.
42. Adachi K, Chung SH, Friedrich H, Buseck PR. Fractal parameters of individual soot particles determined using electron tomography: Implications for optical properties. J Geophys Res-Atmos. 2007;112(D14). https://doi.org/10.1029/2006jd008296.
43. Adachi K, Chung SH, Buseck PR. Shapes of soot aerosol particles and implications for their effects on climate. J Geophys Res-Atmos. 2010;115(D15). https://doi.org/10.1029/2009jd012868.
44. Odhiambo M, Routh J. Does black carbon contribute to eutrophication in large lakes? Curr Pollut Rep. 2016;2(4):236–8. https://doi.org/10.1007/s40726-016-0042-4.
45. Pagels J, Khalizov AF, McMurry PH, Zhang RY. Processing of soot by controlled sulphuric acid and water condensation—mass and mobility relationship. Aerosol Sci Technol. 2009;43(7):629–40. https://doi.org/10.1080/02786820902810685.
46. Xue H, Khalizov AF, Wang L, Zheng J, Zhang R. Effects of coating of dicarboxylic acids on the mass–mobility relationship of soot particles. Environ Sci Technol. 2009;43(8):2787–92. https://doi.org/10.1021/es803287v.
47. Park K, Cao F, Kittelson DB, McMurry PH. Relationship between particle mass and mobility for diesel exhaust particles. Environ Sci Technol. 2003;37(3):577–83. https://doi.org/10.1021/es025960v.
48. Khalizov AF, Lin Y, Qiu C, Guo S, Collins D, Zhang R. Role of OH-initiated oxidation of isoprene in aging of combustion soot. Environ Sci Technol. 2013;47(5):2254–63. https://doi.org/10.1021/es3045339.
49. Rissler J, Messing ME, Malik AI, Nilsson PT, Nordin EZ, Bohgard M, et al. Effective density characterization of soot agglomerates from various sources and comparison to aggregation theory. Aerosol Sci Technol. 2013;47(7):792–805. https://doi.org/10.1080/02786826.2013.791381.
50. Sorensen CM. The mobility of fractal aggregates: a review. Aerosol Sci Technol. 2011;45(7):765–79. https://doi.org/10.1080/02786826.2011.560909.
51. Willeke K, Baron P. Aerosol measurement: principles, techniques, and applications. Van Nostrand Reinhold. 2001. https://doi.org/10.1002/9781118001684.
52. DeCarlo PF, Slowik JG, Worsnop DR, Davidovits P, Jimenez JL. Particle morphology and density characterization by combined mobility and aerodynamic diameter measurements. Part 1: theory. Aerosol Sci Technol. 2004;38(12):1185–205. https://doi.org/10.1080/027868290903907.
53. Han C, Li S-M, Liu P, Lee P. Size dependence of the physical characteristics of particles containing refractory black carbon in diesel vehicle exhaust. Environ Sci Technol. 2019;53(1):137–45. https://doi.org/10.1021/acs.est.8b04603.

54. Qiu C, Khalizov AF, Zhang R. Soot aging from OH-initiated oxidation of toluene. Environ Sci Technol. 2012;46(17):9464–72. https://doi.org/10.1021/es301883y.
55. Liu D, Allan JD, Young DE, Coe H, Beddows D, Fleming ZL, et al. Size distribution, mixing state and source apportionment of black carbon aerosol in London during wintertime. Atmos Chem Phys. 2014;14(18):10061–84. https://doi.org/10.5194/acp-14-10061-2014.
56. Geller M, Biswas S, Sioutas C. Determination of particle effective density in urban environments with a differential mobility analyzer and aerosol particle mass analyzer. Aerosol Sci Technol. 2006;40(9):709–23. https://doi.org/10.1080/02786820600803925.
57. Barone TL, Lall AA, Storey JME, Mulholland GW, Prikhodko VY, Frankland JH, et al. Size-resolved density measurements of particle emissions from an advanced combustion diesel engine: effect of aggregate morphology. Energy Fuel. 2011;25(5):1978–88. https://doi.org/10.1021/ef200084k.
58. Leskinen J, Ihalainen M, Torvela T, Kortelainen M, Lamberg H, Tiitta P, et al. Effective density and morphology of particles emitted from small-scale combustion of various wood fuels. Environ Sci Technol. 2014;48(22):13298–306. https://doi.org/10.1021/es502214a.
59. Qiu C, Khalizov AF, Hogan B, Petersen EL, Zhang R. High sensitivity of diesel soot morphological and optical properties to combustion temperature in a shock tube. Environ Sci Technol. 2014;48(11):6444–52. https://doi.org/10.1021/es405589d.
60. Rissler J, Nordin EZ, Eriksson AC, Nilsson PT, Frosch M, Sporre MK, et al. Effective density and mixing state of aerosol particles in a near-traffic urban environment. Environ Sci Technol. 2014;48(11):6300–8. https://doi.org/10.1021/es5000353.
61. Tavakoli F, Olfert JS. Determination of particle mass, effective density, mass-mobility exponent, and dynamic shape factor using an aerodynamic aerosol classifier and a differential mobility analyzer in tandem. J Aerosol Sci. 2014;75:35–42. https://doi.org/10.1016/j.jaerosci.2014.04.010.
62. Liu H, Pan X, Wu Y, Wang D, Tian Y, Liu X, et al. Effective densities of soot particles and their relationships with the mixing state at an urban site in the Beijing megacity in the winter of 2018. Atmos Chem Phys. 2019;19(23):14791–804. https://doi.org/10.5194/acp-19-14791-2019.
63. Ma Y, Huang C, Jabbour H, Zheng Z, Wang Y, Jiang Y, et al. Mixing state and light absorption enhancement of black carbon aerosols in summertime Nanjing, China. Atmos Environ. 2020;222:117141. https://doi.org/10.1016/j.atmosenv.2019.117141.
64. Zhang F, Li J. Doubling–adding method for delta-four-stream spherical harmonic expansion approximation in radiative transfer parameterization. J Atmos Sci. 2013;70(10):3084–101. https://doi.org/10.1175/jas-d-12-0334.1.
65. Clarke AD, Shinozuka Y, Kapustin VN, Howell S, Huebert B, Doherty S, et al. Size distributions and mixtures of dust and black carbon aerosol in Asian outflow: physiochemistry and optical properties. J Geophys Res-Atmos. 2004;109(D15). https://doi.org/10.1029/2003jd004378.
66. Zangmeister CD, You R, Lunny EM, Jacobson AE, Okumura M, Zachariah MR, et al. Measured in-situ mass absorption spectra for nine forms of highly-absorbing carbonaceous aerosol. Carbon. 2018;136:85–93. https://doi.org/10.1016/j.carbon.2018.04.057.
67. Carrico CM, Bergin MH, Xu J, Baumann K, Maring H. Urban aerosol radiative properties: measurements during the 1999 Atlanta Supersite Experiment. J Geophys Res-Atmos. 2003;108(D7). https://doi.org/10.1029/2001jd001222.
68. Flowers BA, Dubey MK, Mazzoleni C, Stone EA, Schauer JJ, Kim SW, et al. Optical-chemical-microphysical relationships and closure studies for mixed carbonaceous aerosols observed at Jeju Island; 3-laser photoacoustic spectrometer, particle sizing, and filter analysis. Atmos Chem Phys. 2010;10(21):10387–98. https://doi.org/10.5194/acp-10-10387-2010.
69. Chan TW, Brook JR, Smallwood GJ, Lu G. Time-resolved measurements of black carbon light absorption enhancement in urban and near-urban locations of southern Ontario, Canada. Atmos Chem Phys. 2011;11(20):10407–32. https://doi.org/10.5194/acp-11-10407-2011.
70. Ångström A. On the atmospheric transmission of sun radiation and on dust in the air. Geogr Ann. 1929;11(2):156–66. https://doi.org/10.1080/20014422.1929.11880498.
71. Bond TC. Spectral dependence of visible light absorption by carbonaceous particles emitted from coal combustion. Geophys Res Lett. 2001;28(21):4075–8. https://doi.org/10.1029/2001gl013652.
72. Lewis K, Arnott WP, Moosmüller H, Wold CE. Strong spectral variation of biomass smoke light absorption and single scattering albedo observed with a novel dual-wavelength photoacoustic instrument. J Geophys Res-Atmos. 2008;113(D16). https://doi.org/10.1029/2007jd009699.
73. Moosmüller H, Chakrabarty RK. Technical note: simple analytical relationships between Ångström coefficients of aerosol extinction, scattering, absorption, and single scattering albedo. Atmos Chem Phys. 2011;11:10677–80. https://doi.org/10.5194/acp-11-10677-2011.
74. Liu C, Chung CE, Yin Y, Schnaiter M. The absorption Ångström exponent of black carbon: from numerical aspects. Atmos Chem Phys. 2018;18(9):6259–73. https://doi.org/10.5194/acp-18-6259-2018.
75. Moosmüller H, Arnott WP. Particle optics in the Rayleigh regime. J Air Waste Manage Assoc. 2009;59(9):1028–31. https://doi.org/10.3155/1047-3289.59.9.1028.
76. Kirchstetter TW, Novakov T, Hobbs PV. Evidence that the spectral dependence of light absorption by aerosols is affected by organic carbon. J Geophys Res-Atmos. 2004;109(D21). https://doi.org/10.1029/2004jd004999.
77. Russell PB, Bergstrom RW, Shinozuka Y, Clarke AD, DeCarlo PF, Jimenez JL, et al. Absorption Angstrom Exponent in AERONET and related data as an indicator of aerosol composition. Atmos Chem Phys. 2010;10(3):1155–69. https://doi.org/10.5194/acp-10-1155-2010.
78. Giles DM, Holben BN, Eck TF, Sinyuk A, Smirnov A, Slutsker I, et al. An analysis of AERONET aerosol absorption properties and classifications representative of aerosol source regions. J Geophys Res-Atmos. 2012;117(D17). https://doi.org/10.1029/2012jd018127.
79. Kirchstetter TW, Thatcher TL. Contribution of organic carbon to wood smoke particulate matter absorption of solar radiation. Atmos Chem Phys. 2012;12(14):6067–72. https://doi.org/10.5194/acp-12-6067-2012.
80. Lu Z, Streets DG, Winijkul E, Yan F, Chen Y, Bond TC, et al. Light absorption properties and radiative effects of primary organic aerosol emissions. Environ Sci Technol. 2015;49(8):4868–77. https://doi.org/10.1021/acs.est.5b00211.
81. Ganguly D, Jayaraman A, Gadhavi H, Rajesh TA. Features in wavelength dependence of aerosol absorption observed over central India. Geophys Res Lett. 2005;32(13). https://doi.org/10.1029/2005gl023023.
82. Schnaiter M, Horvath H, Möhler O, Naumann KH, Saathoff H, Schöck OW. UV-VIS-NIR spectral optical properties of soot and soot-containing aerosols. J Aerosol Sci. 2003;34(10):1421–44. https://doi.org/10.1016/S0021-8502(03)00361-6.
83. Lack DA, Cappa CD. Impact of brown and clear carbon on light absorption enhancement, single scatter albedo and absorption wavelength dependence of black carbon. Atmos Chem Phys. 2010;10(9):4207–20. https://doi.org/10.5194/acp-10-4207-2010.

84. Day DE, Hand JL, Carrico CM, Engling G, Malm WC. Humidification factors from laboratory studies of fresh smoke from biomass fuels. J Geophys Res-Atmos. 2006;111(D22). https://doi.org/10.1029/2006jd007221.
85. Haywood JM, Shine KP. The effect of anthropogenic sulfate and soot aerosol on the clear sky planetary radiation budget. Geophys Res Lett. 1995;22(5):603–6. https://doi.org/10.1029/95gl00075.
86. Khalizov AF, Xue H, Wang L, Zheng J, Zhang R. Enhanced light absorption and scattering by carbon soot aerosol internally mixed with sulfuric acid. J Phys Chem A. 2009;113(6):1066–74. https://doi.org/10.1021/jp807531n.
87. Cross ES, Onasch TB, Ahern A, Wrobel W, Slowik JG, Olfert J, et al. Soot particle studies—instrument inter-comparison—project overview. Aerosol Sci Technol. 2010;44(8):592–611. https://doi.org/10.1080/02786826.2010.482113.
88. Khalizov AF, Hogan B, Qiu C, Petersen EL, Zhang R. Characterization of soot aerosol produced from combustion of propane in a shock tube. Aerosol Sci Technol. 2012;46(8):925–36. https://doi.org/10.1080/02786826.2012.683839.
89. Bahadur R, Feng Y, Russell LM, Ramanathan V. Impact of California's air pollution laws on black carbon and their implications for direct radiative forcing. Atmos Environ. 2011;45(5):1162–7. https://doi.org/10.1016/j.atmosenv.2010.10.054.
90. Ackerman TP, Toon OB. Absorption of visible radiation in atmosphere containing mixtures of absorbing and nonabsorbing particles. Appl Opt. 1981;20(20):3661–8. https://doi.org/10.1364/AO.20.003661.
91. You R, Radney JG, Zachariah MR, Zangmeister CD. Measured wavelength-dependent absorption enhancement of internally mixed black carbon with absorbing and nonabsorbing materials. Environ Sci Technol. 2016;50(15):7982–90. https://doi.org/10.1021/acs.est.6b01473.
92. Liu S, Aiken AC, Gorkowski K, Dubey MK, Cappa CD, Williams LR, et al. Enhanced light absorption by mixed source black and brown carbon particles in UK winter. Nat Commun. 2015;6(1):8435. https://doi.org/10.1038/ncomms9435.
93. Xie C, Xu W, Wang J, Liu D, Ge X, Zhang Q, et al. Light absorption enhancement of black carbon in urban Beijing in summer. Atmos Environ. 2019;213:499–504. https://doi.org/10.1016/j.atmosenv.2019.06.041.
94. Wang J, Zhang Q, Chen M, Collier S, Zhou S, Ge X, et al. First chemical characterization of refractory black carbon aerosols and associated coatings over the Tibetan Plateau (4730 m a.s.l). Environ Sci Technol. 2017;51(24):14072–82. https://doi.org/10.1021/acs.est.7b03973.
95. Shiraiwa M, Kondo Y, Iwamoto T, Kita K. Amplification of light absorption of black carbon by organic coating. Aerosol Sci Technol. 2010;44(1):46–54. https://doi.org/10.1080/02786820903357686.
96. Saliba G, Subramanian R, Saleh R, Ahern AT, Lipsky EM, Tasoglou A, et al. Optical properties of black carbon in cookstove emissions coated with secondary organic aerosols: measurements and modeling. Aerosol Sci Technol. 2016;50(11):1264–76. https://doi.org/10.1080/02786826.2016.1225947.
97. Knox A, Evans GJ, Brook JR, Yao X, Jeong CH, Godri KJ, et al. Mass absorption cross-section of ambient black carbon aerosol in relation to chemical age. Aerosol Sci Technol. 2009;43(6):522–32. https://doi.org/10.1080/02786820902777207.
98. Lack DA, Langridge JM, Bahreini R, Cappa CD, Middlebrook AM, Schwarz JP. Brown carbon and internal mixing in biomass burning particles. Proc Natl Acad Sci. 2012;109(37):14802–7. https://doi.org/10.1073/pnas.1206575109.
99. Wang Q, Huang RJ, Cao J, Han Y, Wang G, Li G, et al. Mixing state of black carbon aerosol in a heavily polluted urban area of China: implications for light absorption enhancement. Aerosol Sci Technol. 2014;48(7):689–97. https://doi.org/10.1080/02786826.2014.917758.
100. Cui X, Wang X, Yang L, Chen B, Chen J, Andersson A, et al. Radiative absorption enhancement from coatings on black carbon aerosols. Sci Total Environ. 2016;551–552:51–6. https://doi.org/10.1016/j.scitotenv.2016.02.026.
101. Barnard JC, Volkamer R, Kassianov EI. Estimation of the mass absorption cross section of the organic carbon component of aerosols in the Mexico City Metropolitan Area. Atmos Chem Phys. 2008;8(22):6665–79. https://doi.org/10.5194/acp-8-6665-2008.
102. Clarke A, McNaughton C, Kapustin V, Shinozuka Y, Howell S, Dibb J, et al. Biomass burning and pollution aerosol over North America: organic components and their influence on spectral optical properties and humidification response. J Geophys Res-Atmos. 2007;112(D12). https://doi.org/10.1029/2006jd007777.
103. Alexander DTL, Crozier PA, Anderson JR. Brown carbon spheres in East Asian outflow and their optical properties. Science. 2008;321(5890):833–6. https://doi.org/10.1126/science.1155296.
104. Gustafsson Ö, Kruså M, Zencak Z, Sheesley RJ, Granat L, Engström E, et al. Brown clouds over South Asia: biomass or fossil fuel combustion? Science. 2009;323(5913):495–8. https://doi.org/10.1126/science.1164857.
105. Riemer N, Ault AP, West M, Craig RL, Curtis JH. Aerosol mixing state: measurements, modeling, and impacts. Rev Geophys. 2019;57:187–249. https://doi.org/10.1029/2018rg000615.
106. Riemer N, West M, Zaveri RA, Easter RC. Simulating the evolution of soot mixing state with a particle-resolved aerosol model. J Geophys Res-Atmos. 2009;114(D9). https://doi.org/10.1029/2008jd011073.
107. Smoluchowski M. Drei Vorträge über Diffusion, Brown'sche molekular Beweging und Koagulation von Kolloidteilchen. Physik Z. 1916a;17:557–85.
108. Smoluchowski M. Versuch Einer Mathematischen Theorie der Koagulations Kinetis Kolloider Losungen. Z Phys Chem. 1916b;92:129–68. https://doi.org/10.1515/zpch-1918-9209.
109. Riemer N, Ault AP, West M, Craig RL, Curtis JH. Aerosol mixing state: measurements, modeling, and impacts. Rev Geophys. 2019;57(2):187–249. https://doi.org/10.1029/2018rg000615.
110. Koch D. Transport and direct radiative forcing of carbonaceous and sulfate aerosols in the GISS GCM. J Geophys Res-Atmos. 2001;106(D17):20311–32. https://doi.org/10.1029/2001jd900038.
111. Solmon F, Giorgi F, Liousse C. Aerosol modelling for regional climate studies: application to anthropogenic particles and evaluation over a European/African domain. Tellus Ser B Chem Phys Meteorol. 2006;58(1):51–72. https://doi.org/10.1111/j.1600-0889.2005.00155.x.
112. Lauer A, Hendricks J, Ackermann I, Schell B, Hass H, Metzger S. Simulating aerosol microphysics with the ECHAM/MADE GCM – part I: model description and comparison with observations. Atmos Chem Phys. 2005;5(12):3251–76. https://doi.org/10.5194/acp-5-3251-2005.
113. Grell GA, Peckham SE, Schmitz R, McKeen SA, Frost G, Skamarock WC, et al. Fully coupled "online" chemistry within the WRF model. Atmos Environ. 2005;39(37):6957–75. https://doi.org/10.1016/j.atmosenv.2005.04.027.
114. Stier P, Feichter J, Kinne S, Kloster S, Vignati E, Wilson J, et al. The aerosol-climate model ECHAM5-HAM. Atmos Chem Phys. 2005;5(4):1125–56. https://doi.org/10.5194/acp-5-1125-2005.
115. Bauer SE, Wright DL, Koch D, Lewis ER, McGraw R, Chang LS, et al. MATRIX (Multiconfiguration Aerosol TRacker of mIXing state): an aerosol microphysical module for global atmospheric models. Atmos Chem Phys. 2008;8(20):6003–35. https://doi.org/10.5194/acp-8-6003-2008.
116. Vogel B, Vogel H, Bäumer D, Bangert M, Lundgren K, Rinke R, et al. The comprehensive model system COSMO-ART –

Radiative impact of aerosol on the state of the atmosphere on the regional scale. Atmos Chem Phys. 2009;9(22):8661–80. https://doi.org/10.5194/acp-9-8661-2009.
117. Liu X, Easter RC, Ghan SJ, Zaveri R, Rasch P, Shi X, et al. Toward a minimal representation of aerosols in climate models: description and evaluation in the Community Atmosphere Model CAM5. Geosci Model Dev. 2012;5(3):709–39. https://doi.org/10.5194/gmd-5-709-2012.
118. Binkowski FS, Roselle SJ. Models-3 Community Multiscale Air Quality (CMAQ) model aerosol component 1. Model description. J Geophys Res-Atmos. 2003;108(D6). https://doi.org/10.1029/2001jd001409.
119. Wilson J, Cuvelier C, Raes F. A modeling study of global mixed aerosol fields. J Geophys Res-Atmos. 2001;106(D24):34081–108. https://doi.org/10.1029/2000jd000198.
120. Jacobson MZ. Analysis of aerosol interactions with numerical techniques for solving coagulation, nucleation, condensation, dissolution, and reversible chemistry among multiple size distributions. J Geophys Res-Atmos. 2002;107(D19):AAC 2–1-AAC 2–23. https://doi.org/10.1029/2001jd002044.
121. Matsui H, Koike M, Kondo Y, Moteki N, Fast JD, Zaveri RA. Development and validation of a black carbon mixing state resolved three-dimensional model: aging processes and radiative impact. J Geophys Res-Atmos. 2013;118(5):2304–26. https://doi.org/10.1029/2012jd018446.
122. Zhu S, Sartelet KN, Seigneur C. A size-composition resolved aerosol model for simulating the dynamics of externally mixed particles: SCRAM (v 1.0). Geosci Model Dev. 2015;8(6):1595–612. https://doi.org/10.5194/gmd-8-1595-2015.
123. Ching J, Zaveri RA, Easter RC, Riemer N, Fast JD. A three-dimensional sectional representation of aerosol mixing state for simulating optical properties and cloud condensation nuclei. J Geophys Res-Atmos. 2016;121(10):5912–29. https://doi.org/10.1002/2015jd024323.
124. McGraw R. Description of aerosol dynamics by the quadrature method of moments. Aerosol Sci Technol. 1997;27(2):255–65. https://doi.org/10.1080/02786829708965471.
125. McGraw R, Wright DL. Chemically resolved aerosol dynamics for internal mixtures by the quadrature method of moments. J Aerosol Sci. 2003;34(2):189–209. https://doi.org/10.1016/S0021-8502(02)00157-X.
126. McGraw R, Leng L, Zhu W, Riemer N, West M. Aerosol dynamics using the quadrature method of moments: comparing several quadrature schemes with particle-resolved simulation. J Phys Conf Ser. 2008;125:012020. https://doi.org/10.1088/1742-6596/125/1/012020.
127. Zaveri RA, Easter RC, Fast JD, Peters LK. Model for Simulating Aerosol Interactions and Chemistry (MOSAIC). J Geophys Res-Atmos. 2008;113(D13). https://doi.org/10.1029/2007jd008782.
128. Liu L, Mishchenko MI. Effects of aggregation on scattering and radiative properties of soot aerosols. J Geophys Res-Atmos. 2005;110(D11). https://doi.org/10.1029/2004jd005649.
129. Mackowski DW, Mishchenko MI. A multiple sphere T-matrix Fortran code for use on parallel computer clusters. J Quant Spectrosc Radiat Transf. 2011;112(13):2182–92. https://doi.org/10.1016/j.jqsrt.2011.02.019.
130. Liu C. Optical properties of black carbon aggregates. In: Kokhanovsky A, editor. Springer Series in Light Scattering. 2019. p. 167–218.
131. Liu C, Li J, Yin Y, Zhu B, Feng Q. Optical properties of black carbon aggregates with non-absorptive coating. J Quant Spectrosc Radiat Transf. 2017;187:443–52. https://doi.org/10.1016/j.jqsrt.2016.10.023.
132. Wu Y, Cheng T, Liu D, Allan JD, Zheng L, Chen H. Light absorption enhancement of black carbon aerosol constrained by particle morphology. Environ Sci Technol. 2018;52(12):6912–9. https://doi.org/10.1021/acs.est.8b00636.
133. He C. Radiative properties of atmospheric black carbon (soot) particles with complex structures. 2019. p. 219–54.
134. Bauer SE, Menon S, Koch D, Bond TC, Tsigaridis K. A global modeling study on carbonaceous aerosol microphysical characteristics and radiative effects. Atmos Chem Phys. 2010;10(15):7439–56. https://doi.org/10.5194/acp-10-7439-2010.
135. Ghan SJ, Liu X, Easter RC, Zaveri R, Rasch PJ, Yoon J-H, et al. Toward a minimal representation of aerosols in climate models: comparative decomposition of aerosol direct, semidirect, and indirect radiative forcing. J Clim. 2012;25:6461–76. https://doi.org/10.1175/jcli-d-11-00650.1.
136. Nelson J. Test of a mean field theory for the optics of fractal clusters. J Mod Opt. 1989;36(8):1031–57. https://doi.org/10.1080/09500348914551081.
137. Mishchenko MI, Liu L, Travis LD, Lacis AA. Scattering and radiative properties of semi-external versus external mixtures of different aerosol types. J Quant Spectrosc Radiat Transf. 2004;88(1):139–47. https://doi.org/10.1016/j.jqsrt.2003.12.032.
138. Xu Y-l. Electromagnetic scattering by an aggregate of spheres: asymmetry parameter. Phys Lett A. 1998;249(1):30–6. https://doi.org/10.1016/S0375-9601(98)00708-7.
139. Xu Y-l, Gustafson BÅS. A generalized multiparticle Mie-solution: further experimental verification. J Quant Spectrosc Radiat Transf. 2001;70(4):395–419. https://doi.org/10.1016/S0022-4073(01)00019-X.
140. Xu Y-l, Khlebtsov NG. Orientation-averaged radiative properties of an arbitrary configuration of scatterers. J Quant Spectrosc Radiat Transf. 2003;79–80:1121–37. https://doi.org/10.1016/S0022-4073(02)00345-X.
141. Yurkin MA, Hoekstra AG. The discrete dipole approximation: an overview and recent developments. J Quant Spectrosc Radiat Transf. 2007;106(1):558–89. https://doi.org/10.1016/j.jqsrt.2007.01.034.
142. Yurkin MA, Hoekstra AG. The discrete-dipole-approximation code ADDA: capabilities and known limitations. J Quant Spectrosc Radiat Transf. 2011;112(13):2234–47. https://doi.org/10.1016/j.jqsrt.2011.01.031.
143. Brem BT, Mena Gonzalez FC, Meyers SR, Bond TC, Rood MJ. Laboratory-measured optical properties of inorganic and organic aerosols at relative humidities up to 95%. Aerosol Sci Technol. 2012;46(2):178–90. https://doi.org/10.1080/02786826.2011.617794.
144. Bohren CF, Huffman DR. Absorption and scattering of light by small particles. New York: Wiley; 1983.
145. Bruggeman DAG. Berechnung verschiedener physikalischer Konstanten von heterogenen Substanzen. III. Die elastischen Konstanten der quasiisotropen Mischkörper aus isotropen Substanzen. Ann Phys. 1937;421(2):160–78. https://doi.org/10.1002/andp.19374210205.
146. Garnett JCM, Larmor J XII. Colours in metal glasses and in metallic films. Philosophical Transactions of the Royal Society of London Series A, Containing Papers of a Mathematical or Physical Character. 1904;203(359–371):385–420. https://doi.org/10.1098/rsta.1904.0024.
147. Liu C, Lee Panetta R, Yang P. Inhomogeneity structure and the applicability of effective medium approximations in calculating light scattering by inhomogeneous particles. J Quant Spectrosc Radiat Transf. 2014;146:331–48.
148. Liu C, Teng S, Zhu Y, Yurkin MA, Yung YL. Performance of the discrete dipole approximation for optical properties of black carbon aggregates. J Quant Spectrosc Radiat Transf. 2018;221:98–109. https://doi.org/10.1016/j.jqsrt.2018.09.030.
149. Doner N, Liu F, Yon J. Impact of necking and overlapping on radiative properties of coated soot aggregates. Aerosol Sci

Technol. 2017;51(4):532–42. https://doi.org/10.1080/02786826.2016.1275513.
150. Kahnert M. On the discrepancy between modeled and measured mass absorption cross sections of light absorbing carbon aerosols. Aerosol Sci Technol. 2010;44(6):453–60. https://doi.org/10.1080/02786821003733834.
151. Kahnert M. Modelling the optical and radiative properties of freshly emitted light absorbing carbon within an atmospheric chemical transport model. Atmos Chem Phys. 2010;10(3):1403–16. https://doi.org/10.5194/acp-10-1403-2010.
152. Kandilian R, Heng R-L, Pilon L. Absorption and scattering by fractal aggregates and by their equivalent coated spheres. J Quant Spectrosc Radiat Transf. 2015;151:310–26. https://doi.org/10.1016/j.jqsrt.2014.10.018.
153. Litton CD, Perera IE. Modeling the optical properties of combustion-generated fractal aggregates. Fuel. 2014;130:215–20. https://doi.org/10.1016/j.fuel.2014.04.043.
154. Liu F, Snelling D. Evaluation of the accuracy of the RDG approximation for the absorption and scattering properties of fractal aggregates of flame-generated soot. 40th AIAA Thermophysics Conference. 2008. https://doi.org/10.2514/6.2008-4362.
155. Liu C, Xu X, Yin Y, Schnaiter M, Yung YL. Black carbon aggregates: a database for optical properties. J Quant Spectrosc Radiat Transf. 2019;222–223:170–9. https://doi.org/10.1016/j.jqsrt.2018.10.021.
156. Luo J, Zhang Y, Wang F, Wang J, Zhang Q. Applying machine learning to estimate the optical properties of black carbon fractal aggregates. J Quant Spectrosc Radiat Transf. 2018;215:1–8. https://doi.org/10.1016/j.jqsrt.2018.05.002.
157. Scarnato BV, Vahidinia S, Richard DT, Kirchstetter TW. Effects of internal mixing and aggregate morphology on optical properties of black carbon using a discrete dipole approximation model. Atmos Chem Phys. 2013;13(10):5089–101. https://doi.org/10.5194/acp-13-5089-2013.
158. Soewono A, Rogak SN. Morphology and optical properties of numerically simulated soot aggregates. Aerosol Sci Technol. 2013;47(3):267–74. https://doi.org/10.1080/02786826.2012.749972.
159. Wu Y, Cheng T, Zheng L, Chen H. A study of optical properties of soot aggregates composed of poly-disperse monomers using the superposition T-matrix method. Aerosol Sci Technol. 2015;49(10):941–9. https://doi.org/10.1080/02786826.2015.1083938.
160. Filippov AV, Zurita M, Rosner DE. Fractal-like aggregates: relation between morphology and physical properties. J Colloid Interface Sci. 2000;229(1):261–73. https://doi.org/10.1006/jcis.2000.7027.
161. Teng S, Liu C, Schnaiter M, Chakrabarty RK, Liu F. Accounting for the effects of nonideal minor structures on the optical properties of black carbon aerosols. Atmos Chem Phys. 2019;19(5):2917–31. https://doi.org/10.5194/acp-19-2917-2019.
162. Jacobson MZ. Short-term effects of controlling fossil-fuel soot, biofuel soot and gases, and methane on climate, Arctic ice, and air pollution health. J Geophys Res-Atmos. 2010;115(D14). https://doi.org/10.1029/2009jd013795.
163. D'Almeida GA, Koepke P, Shettle E. Atmospheric aerosols global climatology and radiative characteristics. A Deepak publishing. 1991.
164. Wu Y, Gu X, Cheng T, Xie D, Yu T, Chen H, et al. The single scattering properties of the aerosol particles as aggregated spheres. J Quant Spectrosc Radiat Transf. 2012;113(12):1454–66. https://doi.org/10.1016/j.jqsrt.2012.03.015.
165. Zhang H, Zhou C, Wang Z, Zhao S, Li J. The influence of different black carbon and sulfate mixing methods on their optical and radiative properties. J Quant Spectrosc Radiat Transf. 2015;161:105–16. https://doi.org/10.1016/j.jqsrt.2015.04.002.